TRANSITION-METAL-DOPED ALKALI BOROSILICATE GLASS AS A PHOSPHOR MATERIAL

BY

ALADDIN GELEIL

B.S. ALFRED UNIVERSITY (2003)

SIGNATURE OF AUTHOR (Signature on file)

APPROVED BY (Signature on file)
ALEXIS CLARE, ADVISOR

(Signature on file)
SUHAS BHANDARKER, ADVISORY COMMITTEE

(Signature on file)
JAMES SHELBY, ADVISORY COMMITTEE

(Signature on file)
WILLIAM LaCOURSE, CHAIR, ORAL THESIS DEFENSE

ACCEPTED BY (Signature on file)
ALASTAIR CORMACK, DEAN,
KAZUO INAMORI SCHOOL OF ENGINEERING

ACKNOWLEDGMENTS

The author would first like to acknowledge the CES faculty at Alfred University for the opportunity to do this work. I am thankful to have interacted with various professors, from whom I have learned so much. I would first like to thank Dr. Alexis Clare for her inspiration, help, and the laughter we've shared. Additionally, I learned a great deal about glass in general from Dr. James Shelby. I would also like to thank Dr. Suhas Bhandarkar for helping me think about the practical applications of research work, which may often be overlooked. My first year of graduate school turned out to be very fun and informative, thanks to the presence and help of Drs. Bryan Wheaton, Doug Wing, and Matt Hall, as well as Fabienne Raszewski. Other important people in my life include my parents and my two brothers with whom I've shared many good times.

TABLE OF CONTENTS

LIST OF TABLES

Page

LIST OF FIGURES

Page

ABSTRACT

Alkali-borosilicate glasses doped with transition metals were studied to test their suitability as phosphor materials. The goal of this work is to employ a low-processing temperature glass system doped with photoluminescent activators as a direct coating on long-wavelength UV and blue GaN and InGaN LEDs. The blue or UV LED emission would act as the excitation source, so that the combination of emission colors yields white light via additive mixing. The LED materials must be processed at moderate temperatures (approximately $\leq 500°$ C), so a thermally suitable glass host is of importance. The transition metal ions that were studied here are Cr^{3+} and Mn^{2+}, as well as a reduced niobium-containing glass that contains a mix of niobium oxidation states—primarily Nb^{4+} and Nb^{5+}. The green-colored Cr^{3+}-containing glass was found to emit weak red/near IR light upon excitation with 450 nm light. Both Mn^{2+}- and Nb-doped glasses were transparent, and found to emit intense orange light with a peak emission wavelength of around 600 nm upon excitation with 366 nm UV radiation. Niobium in the reduced state [Nb^{4+}] was detected via electron spin resonance [ESR] measurements. Glasses near the base glass composition of 11.7 Na_2O•36.7 B_2O_3•51.6 SiO_2 are known to be spinodally phase-separated on the order of tens of Angstroms, but this was not found to be detrimental to the fluorescence properties. The host glass exhibited onset of glass transition temperature [$T_g \approx 460°$ C] and a coefficient of linear thermal expansion [CTE] of around 4-5 ppm*K^{-1}, which matches the typical LED materials well. The reduced state of manganese was readily obtained via traditional batching and melting techniques, and the Mn^{2+}-doped alkali borosilicate would make a suitable orange-emitting fluorescent material. The luminescence of the niobium-containing glass may also be useful for the orange emission if an appropriate model for the fluorescence were determined. The 600 nm emissions would require the addition of other colors to achieve white light, so a mix of luminescent activators such as rare-earths would be necessary in the proposed phosphor system.

I. LITERATURE SURVEY

A. Luminescence Phenomena

Phosphor materials enable the conversion of one type of incident electromagnetic energy to another.[1] The emitted energy is typically in the form of visible light. Luminescent materials emit visible radiation upon excitation by radiation of higher energies (often short-to mid-wavelength UV), so luminescent materials are often used as phosphors. Devices such as fluorescent lamps, CRTs (televisions), and plasma display panels (PDPs) all employ phosphors of some form or another. A photoluminescent material is one which is excited by electromagnetic radiation (photons) and subsequently emits radiation—other photons—usually of different energy.

Phosphors are solids which convert certain types of energy into electromagnetic radiation in excess of thermal radiation. The electromagnetic radiation emitted by phosphor materials is usually in the visible range, but may also lie in other regions of the spectrum such as the ultraviolet [UV] or infrared [IR].

One of the more common applications of photoluminescent materials is in fluorescent lamps. The lamps consist of a glass tube in which a low-pressure mercury discharge generates ultraviolet radiation (85% of which is the 254 nm short UV emission). The lamp phosphor (or a mix of phosphors) is applied to the inner side of the tube. The phosphors convert the UV radiation into visible (white) light.[1] Conversion of electricity to light is much more efficient in a fluorescent lamp than an incandescent, hence the appeal of fluorescent lighting.

Luminescence phenomena have been studied in a number of solid materials since the early 1900s.[1] There are a few classifications within the term 'luminescence' which implies differing excitation/emission processes. Some of the terminology is summarized in Table I. From the table, it is evident that there are various excitation processes. Those most relevant to this work are fluorescence and phosphorescence, which are subsets of photoluminescent phenomena. The fluorescent lamp phosphors are photoluminescent materials in that they are excited by UV photons of 254 nm wavelength, which results in the

visible emission. For example, the distinction between fluorescence and phosphorescence can be easily observed for a fluorescent lamp in a dark room—after switching the lamp off, there will be a detectable low-intensity glow that continues to be emitted from the bulb for a few seconds. The long decay time of the emission qualifies the material coating the inside of the bulb as a true 'phosphor'.

The present study focused on the development of transition-metal [TM] doped glasses to function as phosphor materials. The goal was to find TM ions that would be excited by blue or UV light, with potential application in glass coatings to create white light from blue LEDs. For the materials described in this work, either long or short decay times are useful. The primary consideration is the excitation of the material by long-wavelength UV or short-wavelength visible photons with subsequent visible and colored luminescence. The term 'phosphor material' may then be applied to one that shows an instantaneous fluorescent emission upon UV/visible excitation. The terms *luminescence* and *fluorescence* are therefore used interchangeably in the present text.

Table I. Summary of Relevant Luminescence Terminology

Designation	Sub set	Means of Excitation	Comment
Photoluminescence	Fluorescence	Low energy photons (UV/Visible light)	Decay time $\leq 10^{-8}$ s
	Phosphorescence	(UV/Visible light)	Decay time $\geq 10^{-8}$ s
Electroluminescence		Electric Voltage	
Cathodoluminescence		Cathode Rays/Electron beams	
Chemiluminescence		Chemical reaction	
Bioluminescence		Biochemical reaction	

We now turn to a description of some of the basic principles of luminescence phenomena. Figure 1 displays a hypothetical luminescent crystal and the corresponding energy level scheme. The system consists of a host lattice

and a luminescent center (the ion **A**) which is termed an activator. Incident electromagnetic radiation raises the ion from the **A** ground state to an excited state denoted as **A'** in Figure 1(b). The excited state subsequently decays back to the ground state to minimize the system's energy. In the energy level diagram below, the **A'** state decays to **A** by a sum of two processes—a radiative transition denoted as **R**, and a non-radiative transition denoted as **NR**. The radiative transitions are the luminesced photons (visible or otherwise), and the non-radiative transitions may be manifested as quanta of lattice vibrations (phonons or heat energy).

Atoms and ions can contain numerous electrons, and it is typically electronic excitations that are responsible for much of the observed and applied phenomena. For example, the excitation of a transition metal cation may involve the movement of an electron from a low energy configuration within a d-orbital to a high energy position in a different d-orbital (d-d transition). Similar situations are seen in rare-earth ions, which contain large numbers of electrons in both d and f orbitals, and consequently display many transitions, including f-f transitions. Luminescence of both transition metal and rare-earth ions is well known in various crystals and, and the phenomena has been used in a number of technologies, including visible and IR lasers, in addition to phosphors.

We may now attempt a deeper understanding of the role of activators in various hosts. Electronic transitions are often coupled with optical phenomena, especially in many of the more complicated atoms of the periodic table. The present study focused on transition metal ions as activators, which requires some contemplation of the d orbitals, and the various energy levels that electrons of TM ions may occupy at ground and excited states.

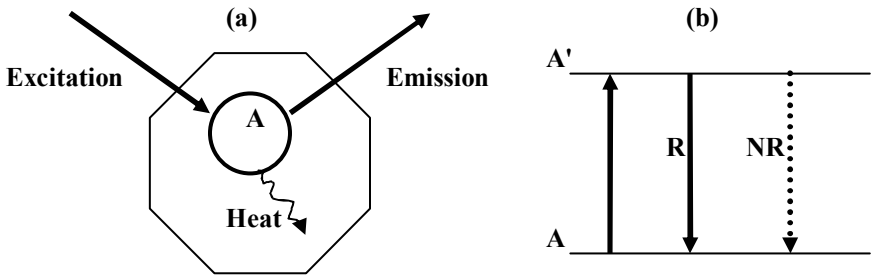

Figure 1. Pictorial representation of a luminescent center. (After Blasse[1]) (a) Shows processes due to the presence of an activator ion within a host lattice. (b) Displays a simplified 2-level energy diagram for the A ion.

B. Electronic Structure of Atoms and Basic Ligand Field Theory

The solution of the hydrogen atom in quantum mechanics has provided insight into the energy levels and distribution of electrons in the various atoms of the periodic table. The well-known results are the descriptions of the electronic orbitals that surround the positive nuclei of atoms.

The appropriate starting point is the specification of electrons in atoms or ions with the well-known quantum numbers. Some contemplation of the specified electronic quantum numbers makes the selection rules for electronic transitions (as in absorption or excitation spectra) more tractable. Four quantum numbers n, l, m_l, and m_s specify the wavefunctions of electrons in atoms. The principal quantum number is called n and refers to the major shell in which the electron is located. n can assume any positive integer value (n = 1, 2, 3, 4, 5, etc.). l is referred to as the subshell or orbital angular momentum quantum number, and denotes the subshell where the electron is located; l may have values ranging from 0 to n-1 (l = 0, 1, 2, ...n-1). The quantity m_l is referred to as the azimuthal or magnetic quantum number, and is the z component of the electron's angular momentum. The values of m_l range from +l to –l. We can see that for l = 2 (d-shell electron), we have 5 values for m_l: -2, -1, 0, 1, 2. The m_s number is a byproduct of relativistic quantum mechanics, and refers to the 'spin' of an

electron. The m_s number can only attain 2 values: either +1/2 for positive spin, or -1/2 for negative spin.

It is the last three quantum numbers that are of most concern to experimentalists. It is possible, for example, to directly investigate spin states in techniques such as electron spin resonance [ESR]. The states of atoms are specified with specific terminology in spectroscopic notation, which is discussed further below.

The orbitals of most concern for the first and second row transition elements are the s, p, and d orbital configurations. The f-orbitals of rare-earth elements (lanthanides and actinides) also display a great deal of technologically important and interesting behavior, but their configurations are a great deal more complex, and so will not be discussed here. The reader is referred to the text of L.E. Orgel for the basics of ligand field theory or that of C.J. Ballhausen for a full quantum-mechanical treatment of the subject.[2,3] A good treatment of TM ions in glass is given by A. Paul in *Chemistry of Glasses*.[4] One can easily note the angular dependence of the wave-functions for the s, p, and d electrons, as shown in Figures 2 and 3. The s orbital displays spherical symmetry about the origin, so variation of the wave function with distance from the nucleus is independent of the direction. The p and d orbitals demonstrate preferred directions, which become important considerations depending on whether the ion in question is free or bounded by attached chemical groups (ligands). A transition metal ion bound in a solid will also experience differences in its local environment due to different possibilities in anion coordination (i.e. octahedral or tetrahedral). The behavior of the d orbitals in presence of fields is treated by crystal field theory (ligand field theory) or molecular orbital theory. The molecular orbital theory is more advanced, and will not be discussed here.

There are several consequences when an ion is bound by ligands. The electrostatic crystal-field theory developed by Bethe and Van Vleck is the most basic of arguments, and a decent approximation.[3] A compound such as a metal halide or transition-metal salt is considered to consist of totally ionic bonding, so that the many electrons interact electrostatically, but covalent bonding is

completely neglected.[3] To begin with, consider a positively-charged transition metal ion that is 6-fold coordinated with a regular octahedron of negatively-anions. The anions may be dipolar molecules such as H_2O, so their negative ends would point toward the central ion. Other coordination anions may be O^{2-} or halides F^-, Cl^-, etc. Recall that the electronic orbitals all contain negative charge density for both cations and anions. The negatively-charged d-orbitals have directionality with respect to the x,y, and z axes, and thus with the negatively-charged octahedron that now surrounds them. The interaction can simply be viewed as repulsion between the negatively-charged distributions that line up directly, so these orbitals are left at a higher energy than initially. Conversely, orbitals that are not in direct alignment with the anions of the octahedra are brought to a lower energy state.

A more detailed explanation of the above argument is helpful. The six anions of the octahedron lie along the z axis, and in the x-y plane, as shown in Figure 4. From symmetry, the ligands along the z axis influence the $d_{x^2-y^2}$ and d_{xy} orbitals in the same manner,[3] since neither of these two orbitals are in-line with the z axis. The situation is different for the ligands in the x-y plane, as the directions of maximum charge density of the $d_{x^2-y^2}$ orbitals point at the ligands along the x and y axes, and the directions of maximum charge density for the d_{xy} orbitals point toward the bisectors of the angles between the bond directions to maintain a maximum separation from the ligands.[3] The ligands as well as the orbitals are negatively charged, so an electron in the $d_{x^2-y^2}$ orbital must be repelled more strongly (electrostatically) by the ligands than an electron placed in the d_{xy} orbital. The result is that the addition of an octahedral arrangement of ligands destabilizes both the $d_{x^2-y^2}$ and d_{xy} orbitals, but $d_{x^2-y^2}$ is affected to a greater extent.[3]

Next consider the effect of the octahedron on the d_{xz} and d_{yz} orbitals. These orbitals have the same spatial orientation with respect to ligands in the x-z and y-z planes as the d_{xy} orbital does with ligands in the x-y plane, so the d_{xz} and d_{yz} must be degenerate with the d_{xy} orbital. The situation for d_{z^2} and $d_{x^2-y^2}$ orbitals is not intuitive, since both orbitals contain high charge density along the axes of

the ligands, and so interact strongly with the ligands. The result is that both the d_z^2 and $d_{x^2-y^2}$ orbitals are unstable relative to the d_{xy}, d_{xz} and d_{yz} orbitals when placed in the octahedral ligand environment. In fact, calculations based on group theory show that the the d_z^2 and $d_{x^2-y^2}$ orbitals are *degenerate* when placed in an octahedral environment.[3] Degeneracy refers to separate states being at equivalent energy levels. A proper example are the p_x, p_y, and p_z orbitals which are equivalent except for their respective directions, so the three orbitals are said to be degenerate.

The result is that in a regular octahedral environment, the five d orbitals split into two groups: one group that is the d_{xy}, d_{xz}, and d_{yz} orbitals, and the other group contains the $d_{x^2-y^2}$ and d_z^2 orbitals. The d_{xy}, d_{xz}, and d_{yz} orbitals have their energy levels displaced slightly downward the same amount, since none of them have their maximum electronic density pointing directly at any of the ligands. The d_{xy}, d_{xz}, and d_{yz} orbitals are said to be degenerate with each other. On the other hand, and in contrast to the situation of a free atom, the $d_{x^2-y^2}$ and d_z^2 orbitals have their energy increased by the same amount when made to interact with the octahedron, due to the alignment of the orbital and anion charge densities. The $d_{x^2-y^2}$ and d_z^2 are also degenerate with each other in the regular anion octahedral configuration. The above situations are shown in Figure 4. For the situation of the regular octahedron and from symmetry considerations, the group of d_{xy}, d_{xz}, and d_{yz} are denoted as the t_{2g} orbitals, while the $d_{x^2-y^2}$ and d_z^2 are referred to as the e_g orbitals.

The opposite situation exists for the interaction of d orbitals with a tetrahedral ligand field. Figure 5 shows the five d orbitals in the presence of a regular tetrahedral arrangement of anions (ligands). As in the situation for the octahedron, instabilities arise due to any proximity or overlap in space of the areas of maximum charge density for the orbital and the anion. This time there are larger instabilities for the d_{xy}, d_{xz}, and d_{yz} orbitals, all of which have proximity to one of the anions. Comparing the position of the d_{xy} orbital with the $d_{x^2-y^2}$ orbital, it is evident that each lobe of the d_{xy} orbital has some alignment with one of the

ligands, but the $d_{x^2-y^2}$ orbital has charge density which lies along the bisectors of the angles between ligands, so $d_{x^2-y^2}$ is repelled less than the d_{xy} orbital.[3]

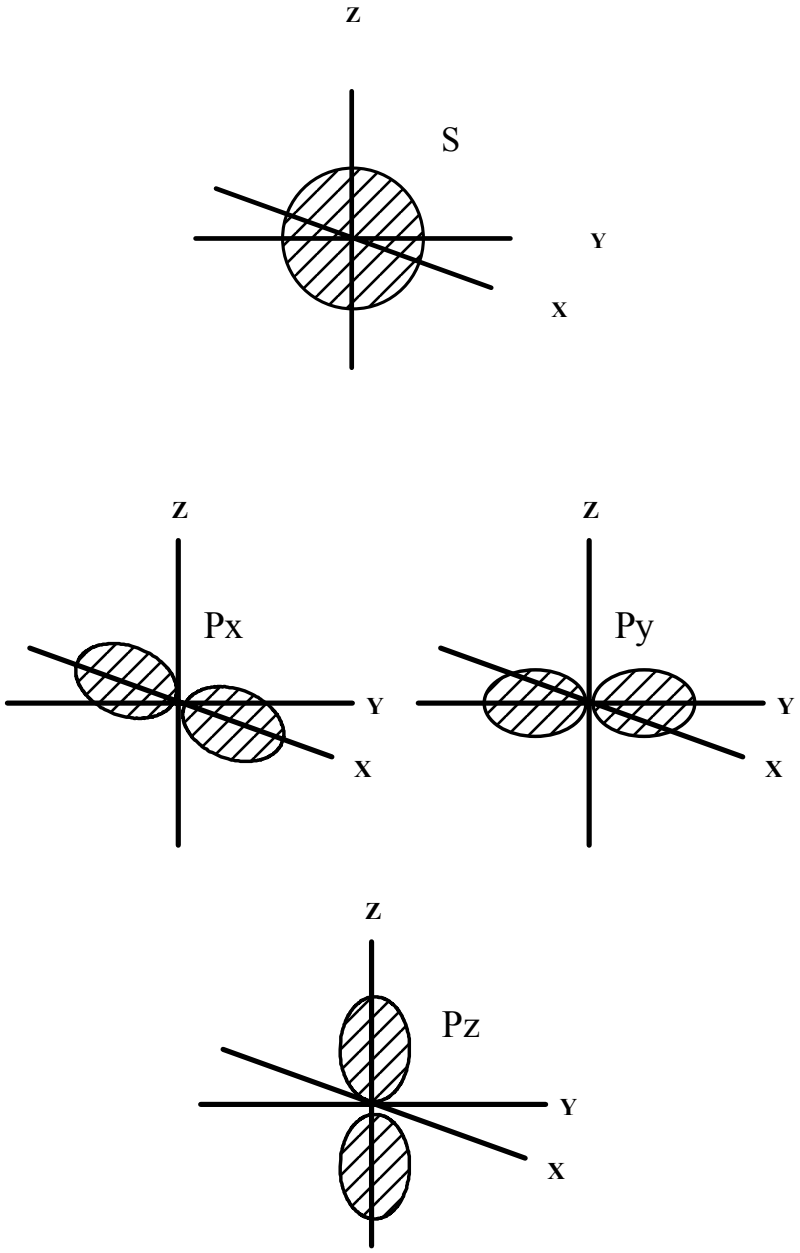

Figure 2. Schematic of s and p orbitals. The orbital shape approximates the space where the electrons are most likely to be found.

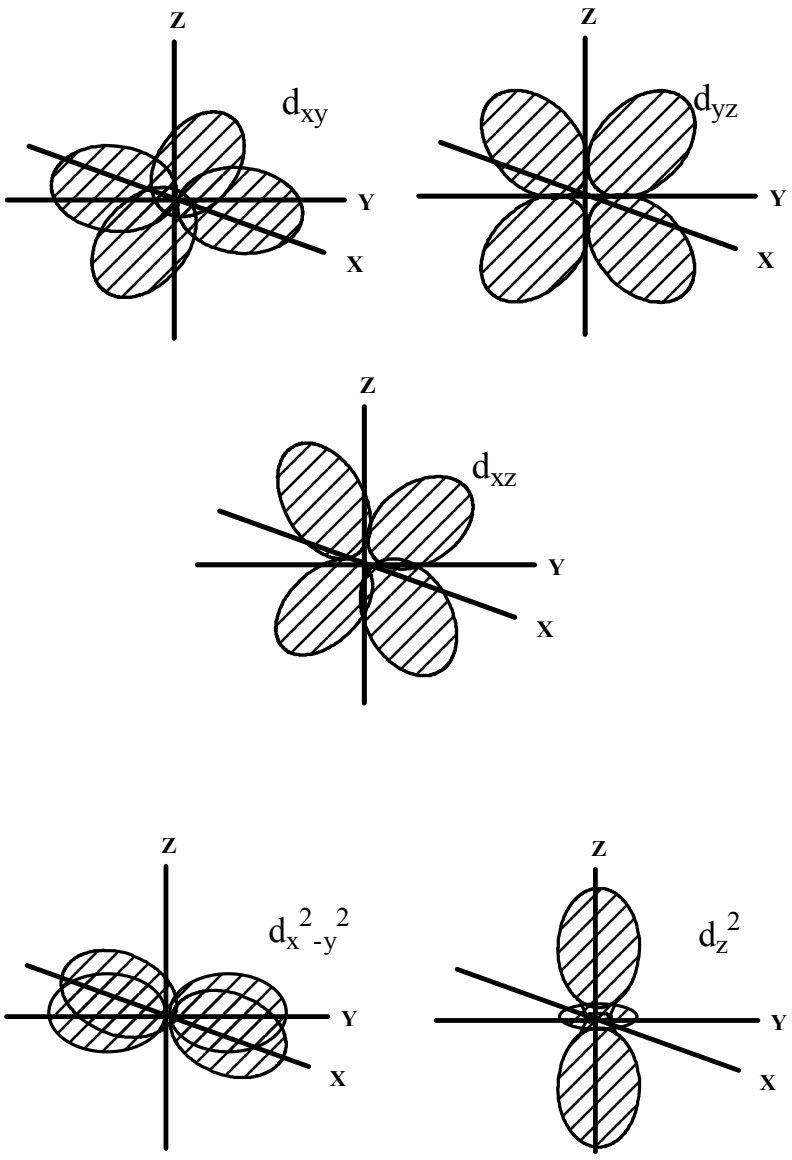

Figure 3. Schematic of d orbitals. The orbital shapes are approximate in all figures.

As in the octahedral case, symmetry arguments dictate that the energy levels of the orbitals will again split, but the greater instability is seen in the d_{xy}, d_{yz}, and d_{xz} orbitals, so that their energy levels are shifted up slightly, and they are the first group of degenerate orbitals. Conversely, the $d_{x^2-y^2}$ and d_{z^2} orbitals are more stable in the tetrahedral arrangement, their energy is shifted downward, and

they are the second group of degenerate orbitals for the tetrahedral arrangement of ligands.[3]

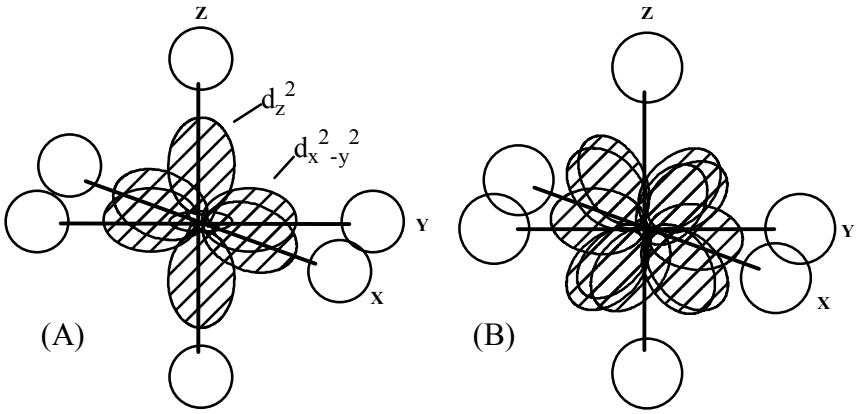

Figure 4. The d orbitals within a regular octahedron of ligands. (A) represents the d_z^2 and $d_{x^2-y^2}$ orbitals, and (B) the The d_{xy}, d_{xz}, and d_{yz} orbitals. The open circles represent the ligands. The $d_{x^2-y^2}$ orbitals point directly along the x and y axes, and the d_z^2 orbital features two lobes that lie directly along z, as well as a small toroid of charge density centered about the origin. The orbitals in (B) do not point directly at any of the ligands, so the effect of the regular octahedron of anions is that these three orbitals to be degenerate with respect to each other.

The resulting arrangement features a positively charged central metal ion surrounded by ligands which impart fields of differing symmetry depending on the configuration. The field (approximated as electrostatic) that is set up by the cation/ligand combination is known as the ligand field or crystal field. The arguments presented offer a decent depiction, but the full quantum-mechanical treatment requires group theoretical arguments and treatment of the various wavefunctions in higher-order perturbation theory, which are outside the scope of this work.

The effect of the described orbital/ligand interaction is manifested in a shift in the energy levels of the d orbitals for coordinated species compared to the energy levels of the orbitals for the free atom or ion. We see the shift in energies as a splitting between energy levels. The subsequent energy difference is called the crystal-field or ligand field splitting, and is often denoted as Δ or 10Dq.

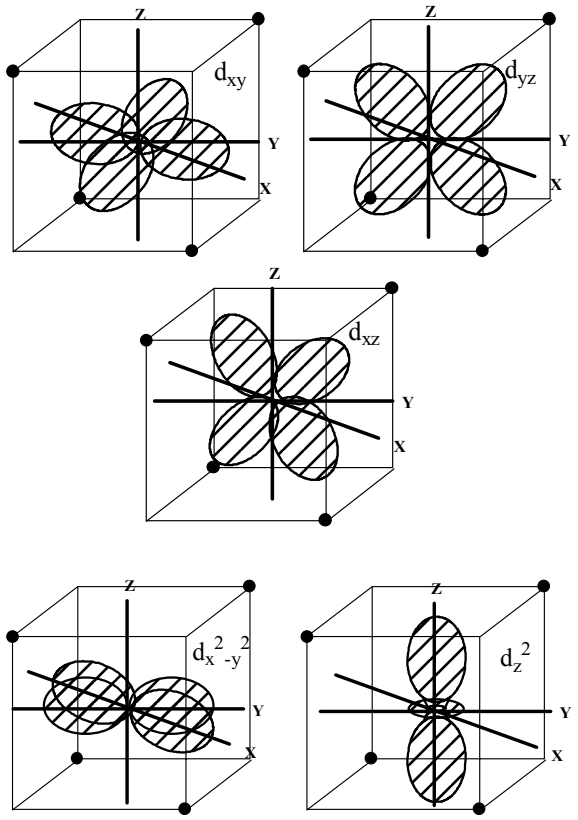

Figure 5. Representation of d_{xy}, d_{xz}, d_{yz} orbital interaction with tetrahedral arrangement of ligands. The black dots represent the negatively-charged ligands.

The Δ parameter is indicated by the differences in energy levels shown in Figure 6. In the case of the square planar complex (c), the $d_{x^2-y^2}$ orbital lobes are taken to point almost directly at the square-planar arrangement of ligands, so they are the least stable in this configuration, and subsequently are at the highest energy level.[3] It is also evident that the d_{z^2} orbital interacts least with the square-planar arrangement, so d_{z^2} is the most stable, and at lowest energy. The same type of splitting between two degenerate levels is not seen in (c), since the interactions are different for the d_{xy}, d_{xz}, and d_{yz} orbitals (but d_{xz} and d_{yz} are degenerate with each other).

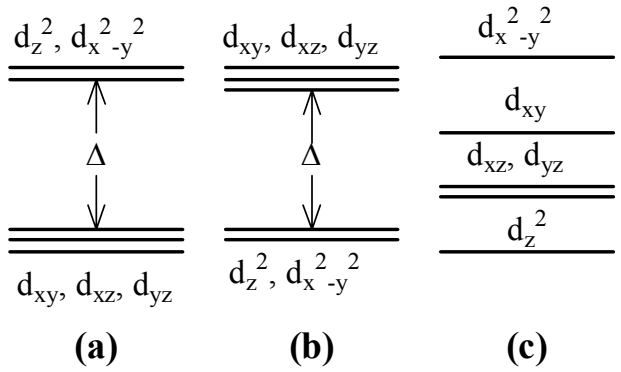

Figure 6. Energy level schemes for d-orbitals in (a) octahedral field, (b) tetrahedral field, and (c) square planar configuration. The reader may infer the correctness of each case in the above diagram from the same symmetry arguments described for the octahedral ligand field (a). After Orgel.[3]

C. Transition Terminology and Selection Rules

The theoretical ligand field and molecular orbital theories give results which agree with each other, and correlate well to the observed absorption spectra (electronic transitions) for ions in solutions, crystals, and glasses. The terms used in interpreting such spectra require some further explanation. For multi-electron atoms with unfilled-shells (such as the first row of transition metal ions), there are usually several ways in which to place electrons in the orbitals, but they are energetically non-equivalent.

The angular momentum and spin multiplicity of an atom are specified by a symbolic representation. The angular momentum of atoms is denoted by the L quantum number, and the spin quantum number becomes S, which is the summation of all electron spins in the ion/atom. Atoms in S, P, D, F states have the same angular momentum L as the Hydrogen atom with a single electron in s, p, d, f, so states with L = 0, 1, 2, 3, 4, 5,..... gives S, P, D, F, G, H respectively. The number of M_s values is called the spin multiplicity. For a state with S = 1, the spin multiplicity is 3 since there are three M_s values: 1, 0, and -1.

The spin multiplicity is given by 2S+1 and is denoted as a left superscript to the notation for L. Some examples are helpful:

For $M_L = 4$, $S = ½$, the symbol is ^2G

For $M_L = 2$, $S = ½$, the symbol is ^2D

For $M_L = 0$, $S = 5/2$, the symbol is ^6S

Spin multiplicities of 1, 2, 3, 4, are called singlets, doublets, triplets, quadruplets, etc. respectively. Above we would have doublet G, doublet D, and sextuplet S.

Russell-Saunders coupling may also take place between spin and angular momentum, which results in the new quantum number for the entire atom J, where J = L+ S. If required, J is indicated as a right subscript to L. The term symbols take the form:

$$^{(2S+1)}L_J \qquad (1)$$

For a ^4D state, one may see $^4D_{7/2}$ for L =2, $M_S = 3/2$, and J = 7/2.

Ground states of atoms or ions may be specified in this way. The ground state of carbon, for example would be $^3P_0$ or ^3P. The ground state is configured $1s^2\ 2s^2\ 2p^2$. The two s shells are filled so that all spins are paired and S = 0. The angular momentum cancels out in the filled shells so that L = 0. The primary consideration are the $2p^2$ electrons.

$$M_L = \Sigma m_l = 0, \text{ so } M_L = \pm 1, \pm 2, \ldots . \pm L$$

$$M_S = \Sigma m_s, = \pm 1/2, \text{ so } M_S = S, S\text{-}1, S\text{-}2, \ldots -S$$

For the ground state of carbon, L = 1, S = 1, so ^3P is the ground state term symbol. Another point concerns the addition of a g or u subscript to a state such as $^6A_{1g}$ (^6S). The g and u refer to the German word *gerade* (even) and *ungerade* (odd) indicate the presence or absence of a change in sign of the wavefunction on inversion through a center of symmetry.[5] The total multiplicity is given by the product (2S +1)(2L +1).

Electronic transitions occur according to specific selection rules, which deal with the changes in quantum numbers between states. The rules are not totally strict guidelines, however, as coupling between various phenomena results in some deviations. There is no restriction on the n quantum number. For the

spin selection rule, $\Delta S = 0$, so that transitions may occur from singlet to singlet, or triplet to triplet states, etc., but changes in spin multiplicity are *forbidden*. The forbidden transitions are generally very weak or absent. J and L can vary by 0, +1, or -1, but transitions J = 0 to J = 0 are also forbidden. The Laporte selection rule forbids u --> u or g --> g transitions, so they are often weak. Transitions known as charge-transfer transitions are g --> u or u --> g, so they are often quite strong.[5] It would seem that the allowed transitions are then s --> p, p --> d, d --> f, and the forbidden transitions s --> s, p --> p, d --> d, s --> d, p --> f. However, spin-forbidden transitions may still be observed due to spin-orbit coupling and vibronic coupling.[5] It is evident that the situation can become quite complex, and only the basic ideas are presented here to give the reader an introduction to the lexicon of transitions. The consideration of ions such as rare-earths involves many more electrons, and many more possibilities for radiative and non-radiative decay, charge transfers, and various coupling mechanisms. The general arguments presented here offer a basic introduction, but specific phenomena would require equally specific and involved studies.

The above principles are seen in the appropriate energy level diagrams, which have been calculated by a number of authors.[3,6] As an example, consider a d^1 ion such as Ti^{3+}. The d^1 configuration results in only two electronic states in octahedral coordination, as shown in Figure 7: the ^2E upper level, and the $^4T_2$ lower level.[7] Additionally, one may apply what is known as 'hole formalism' to deduce that a d^9 configuration is inverted relative to the d^1 configuration.[4] Also inverted with respect to each other are the d^2 with d^8; d^3 with d^7; and d^4 with d^6 configurations.

Single crystals of Al_2O_3:Ti^{3+} are in laser materials. The absorption band corresponds to $^4T_2$--> ^2E, and the ^2E--> $^4T_2$ transition is the emission band. One should note that the separation between levels increases with increasing Δ, which is plotted on the horizontal axis of Figure 7. The emission properties vary depending on the ligand field strength of the host. The three most-studied matrix materials for Ti^{3+} as the lasing ion are $YAlO_3$, Al_2O_3, and $BeAl_2O_4$, which all result in Ti^{3+} in octahedral symmetry.[7] The Ti^{3+} ion offers a broad range of

tunability of the emission in alumina (≈ 660 nm-1.0μm) and beryl aluminate (≈ 720 nm-950 nm).[7]

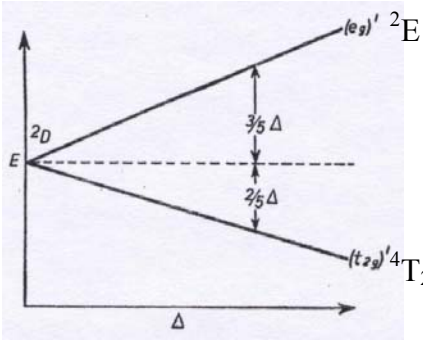

Figure 7. Energy level diagram for d^1 configuration. The upper level has a magnitude equal to 3/5 of the total energy, whereas the lower level contains the other 2/5.

The magnitude of the crystal field splitting gives insight into the environment of the ion in question. The correct crystal field and energy level calculations are well known in the literature.[3,6]

Experimentally, the crystal field parameters may be determined from absorption spectroscopy, electron spin resonance [ESR], or other techniques. The energy matrices for the various levels have been specified by Sugano et. al.,[6] so ligand field parameters may be calculated by setting the appropriate matrices equal to the energies observed in the absorption spectrum.[6] The observed crystal field parameters may then be compared to what is predicted by group theory.

The energies of different states were calculated via group theory by Racah, who expressed them in terms of the parameters A, B, and C. Usually only the latter parameters B and C are necessary to describe the relative separation of energy levels, since the A parameter shifts all levels of an ion equally.[4] In general, the Racah B parameters for ions with high Dq values tend to be low, which indicates a high degree of covalent bonding.[4,6,8,9] The apparent B value in complexes is always smaller than that of the free ion—this phenomenon is known as the nephelauxetic effect and is attributed to delocalization of the metal electrons over molecular orbitals that encompass not only the metal but the

ligands as well. The result of this delocalization ('cloud expansion') is that the average interelectronic repulsion is reduced and B is smaller for the complexed ion. The situation in glasses does not seem to correspond to the regular bonding arrangements of complexes, so the ligand field parameters may give qualitative indications of the TM ion's environment only. When an ion is dissolved in a glass, the effect on the B parameter is difficult to interpret.

Values of Racah parameters for the free ions of the iron group may be determined directly from spectroscopic data. If the data are unavailable, it is possible to interpolate or extrapolate from data that have been found experimentally.[6] For qualitative comparison, values of Racah parameters B and C for free ions are given in Table 2.

Table II. Racah parameters for free transition metal ions. From Sugano, et. al.[6]

Ion	B (cm^{-1})	C (cm^{-1})	Ion	B (cm^{-1})	C (cm^{-1})
Ti^{2+}	695	2910			
V^{2+}	755	3257	V^{3+}	862	3815
Cr^{2+}	810	3565	Cr^{3+}	918	4133
Mn^{2+}	860	3850	Mn^{3+}	965	4450
Fe^{2+}	917	4040	Fe^{3+}	1015	4800
Co^{2+}	971	4497	Co^{3+}	1065	5120
Ni^{2+}	1030	4850	Ni^{3+}	1115	5450

The preceding paragraphs make numerous simplifying assumptions concerning the environment of the ion in question, but turn out to be a worthwhile discussion with regard to the role of these types of ions in most glass systems. The bonding is assumed to be totally ionic, which is fairly valid for the interaction between alkali and other metal cations with O^{2-} ions in glasses. Transition metal ions are said to be present in oxide glass structures within coordination 'polyhedra'. There have been numerous studies to suggest that transition metal ions such as Mn^{2+} and Cr^{3+} attain approximately octahedral coordinations in oxide

glasses of various compositions, including silicates and phophates.[4,8-14] The actual role of the transition metal ions in the structure (i.e. as network formers, intermediates, or modifiers) is less clear, however.

D. Transition Metals

The transition metals occupy the majority of the periodic table. The transition metals are the atoms whose d-shells get filled with electrons from left to right across the fourth and fifth rows. The first row starts with scandium [Sc], which features an [Ar] $3d^1 4s^2$ electronic configuration. The next atom in the sequence is titanium [Ti] with the [Ar] $3d^1 4s^2$ configuration. One should note that to the left of Sc is calcium [Ca] which has a full outer shell, but 0 d electrons ([Ar] $3d^0 4s^2$ configuration). As row 4 is traversed from left to right, we see the sequence Sc, Ti, V, Cr, Mn, Fe, Co, Ni, Cu, Zn, and the d-shell gets filled completely. The fifth row features atoms whose 3d shells are full, but whose 4d shells start to become filled with electrons. The fifth row starts with yttrium and its [Kr] $4d^1 5s^2$ configuration: one can also note the full outer shell ($5s^2$). We see the sequence Y, Zr, Nb, Mo, Tc, Ru, Rh, Pd, Ag, and Cd, so that the 4-d shell gets filled completely. Historically, the great interest in the transition metal atoms is connected to their ability to form compounds in which the outermost set of five stable d electron orbitals is only partially filled. It is the presence of incomplete d-electron shells which is responsible for many of the visible colors of crystals and minerals, and also for the paramagnetic properties that many transition metal compounds display.[5]

The d orbitals of transition metals behave in various ways depending which chemical species they are surrounded with, and in what configuration. As an example, we may consider an aqueous ion such as $[Mn(H_2O)_6]^{2+}$. Manganese is in the Mn^{2+} state with a $3d^5$ configuration, and the ion is coordinated octahedrally by 6 neutral H_2O molecules—hence the resultant 2+ charge. The 3-d shell contains one electron in each of the five possible orbitals (d_{xy}, d_{xz}, d_{yz}, d_z^2, $d_{x^2-y^2}$) due to Hund's rule of maximum multiplicity; i.e. the d-shell contains five unpaired electronic spins which result in the ground state of $^6A_{1g}$ or ^6S for the Mn^{2+} ion. The Orgel diagram for the d^5 configuration is given in Figure 8.

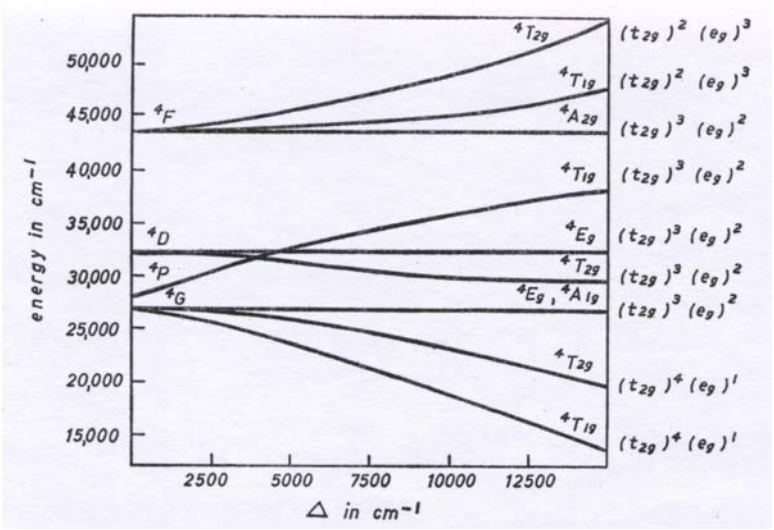

Figure 8. Energy level diagram for d^5 configuration.[3] The ^6S ground state is taken to be at zero energy.

The arguments outlined above can now be used to interpret the absorption spectrum of Mn^{2+}, except for a few details. We see that with respect to the ground state, transitions to the excited states involve changes in the spin multiplicity, which are said to be forbidden.

The selection rules are often relaxed. Coupling of spin and orbital angular momenta does occur, which makes it impossible to divide the wave functions accurately into spin and orbital wave function products.[4] This means that 1) the spin selection rule is not completely valid, and spin-forbidden bands do occur, but are usually of weak intensity. The intensity of these bands increases as spin-orbit coupling constants increase, in particular when moving from left to right in the TM series, and traversing from the first to the third series.[4] 2) The Laporte selection rule is also relaxed because the presence of molecular vibrations in complexes allows coupling to occur between electronic and vibrational energy levels in both the ground and excited states. It is likely, then, that a g (even) electronic level will be combined with a u (odd), and the resultant vibronic level will be u (odd). It is almost certain that both the ground and excited states have both g and u components in their energy levels. 3) If there are forbidden bands

that lie very near in energy to a fully-allowed transition, there is generally a vibrational level which combines the forbidden and allowed bands. The result is that the intensity of the forbidden band is increased—such allowed levels are normally charge transfer bands. 4) There are also excited states that exist whose wavefunctions are combinations of d and p wavefunctions, which results in a u wave function. Transitions are then possible between the g ground states composed of d and p wave functions. 5) There are also distortions from ideal octahedral symmetry. There may be elongation or compression along the z-axis, for example, so that absorption properties are anisotropic, and the resulting absorption is polarized.[4]

An additional consideration of transition metal and inorganic chemistry is the effect of strong or weak ligand fields on the spin states of the metal ion's electrons. Consider Mn^{2+} ion as an example: in octahedral field, the energies of the two sets of orbitals t_{2g} and e_g are separated by the value of ligand field splitting (10Dq or Δ). If there were one electron in each of the five orbitals, each is unpaired, and the resulting ion/ligand combination is known as a high-spin complex. However, the two electrons that should occupy the higher energy e_g orbitals may be forced to occupy the lower-energy t_{2g} orbitals, pair with two of the resident t_{2g} electrons, and assume opposite spins. The reason is purely energetic: the energy of pairing the two electrons into the lower orbitals must be less than having the two electrons occupy the higher energy e_g orbitals caused by the crystal field splitting; the magnitude of the spin-pairing energy must be less than that of the ligand field splitting.

E. Phosphor Materials

Light-emitting diodes [LEDs] are being used more and more frequently for illumination purposes. Commercial LED lighting employs LEDs of various emission wavelengths in combination with phosphor materials to achieve desired lighting characteristics. LEDs feature high efficiency (conversion of electric to light energy), operate at very low current (less demand on power-generation systems), and have long life. LED lighting could replace traditional forms of indoor lighting due to the potential energy savings.

Current LED phosphors are crystalline powders that may be applied as coatings via slurries or electrophoretic deposition, for example.[15] An image of the arrangement is shown in Figure 9. The granular nature of the phosphors requires precise deposition tolerances, which may be difficult to achieve. Characteristics such as particle size are of primary importance. Other features of the phosphor such as are packing density, layer thickness, and uniformity are not easily controlled by slurry-deposition techniques.[15] The result is that light scattering is uncontrolled and leads to undesirable optical effects.

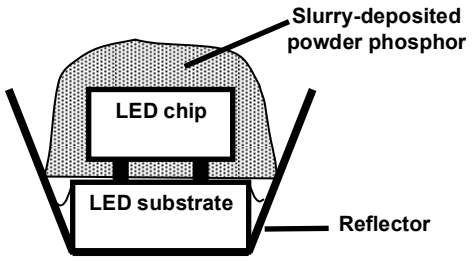

Figure 9. Image of granular phosphor coating on LED die and substrate.

The luminescence of rare-earth doped crystals and glasses is well known, and rare-earth luminescence is characterized by high efficiency. Rare earths have been the main component of laser glasses for many years. A combination of rare-earth phosphors has been used (such as Y_2O_3:Eu for red, YAG:Ce for yellow, and (La,Ce)PO_4:Tb^{3+} for green) to achieve color rendering fluorescent lamps. The spectra of such phosphors feature narrow excitation and emission peaks, so color rendering requires a mix of different activators (to achieve white light, for example).

In contrast to rare-earth activated luminescence, the emissions of transition metal activators are characterized by broad bands. The broad luminescence of such activators would improve the color rendering of a luminescent material. This work focused on transition metal ions as glass dopants since their emissions feature broad emission peaks. The high emission widths may be due to coordinational asymmetry, vibronic coupling, or some other interaction.

Luminescence of transition metal ions upon short-wave UV excitation has been observed in a number of glasses including silicates, phosphates, and borates.[8-12,14,16,17] Low T_g glass systems may be suitable hosts for transition metal ion activators. The idea is to simplify fabrication processes by directly coating GaN or InGaN blue LEDs with the glass phosphor so as to shift the blue spectrum of the LED to a white color which is suitable for indoor use (color temperature ≈ 5000-6000 K). A low-T_g melt is desired because many of the LED die and substrate materials can be compromised if heated above 400° C. A transparent or semi-transparent glass could also spread the beam by lensing, and reduce undesirable color halos in the emission.

This work was begun as an outcome of investigations by K.J. Lynch into the luminescence behavior of several ionic dopants in zinc borosilicate glasses.[17] The ultimate goal of his work was use of the system in an electroluminescent device for solid-state lighting. Lynch's study focused on the use of Cr^{3+}, $Mn^{2+/3+}$, and Eu^{3+} as ionic dopants. The present study was limited to first and second row transition metals, so rare earth ions such as Eu^{3+} were not examined in this work, however, Cr^{3+} and Mn^{2+} provided an appropriate starting point.

The blue and near UV LEDs offer advantages as excitation sources because their emission is of higher energy than the visible wavelengths. It is likely that some activators could be excited by a short-wavelength blue/violet emission, and almost certainly by mid to near UV emission. The mid-to-long wavelength UV LEDs are also becoming more common, and feature emissions with wavelengths that may range from 340 to 390 nm. The goal of this work was to find ions that could be excited by blue light (roughly 400-450 nm), or long wavelength UV (350-390 nm) and emit red, green, or yellow. Subsequent combination of the colored emissions with the remnant blue light from the LED should produce a white light according to additive color mixing. There are some activators that are known to emit blue light upon short-wave UV excitation (Cu^{+} for example), but these activators were not regarded in this study. Excitation of the proposed phosphors by long-wavelength UV would not require the

consideration of any remnant blue light in the emission of the LED/phosphor combination, but would require the use of a blue emitter in the phosphor.

Processing characteristics of the proposed system are important, and require the use of numerous characterization techniques to study glasses as host materials and the activity of TM ions within. The onset of glass transition [T_g] and coefficient of thermal expansion [CTE] are useful for determining the thermal properties of the host glass. These characteristics may be devised from differential scanning calorimetry [DSC] and dilatometry respectively.

The states of ions in the glass may be inferred from spectroscopic methods. The relevant opto-electronic transitions can be resolved in absorbance and fluorescence spectroscopy. The study and detection of transition metal ions in various glass systems has been also been facilitated by the use of electron spin resonance spectroscopy [ESR], or electron paramagnetic resonance [EPR].

ESR is a useful technique for glasses because of its high sensitivity and distinct spectrum for each species examined, including not-so-frequent isotopes. It is fortunate that the coupling between spin and angular momentum in solids is minimized because of the quenching of the angular momentum—the same situation holds in glasses—so that the spin states of electrons are left 'pure', and the ion-ligand combination may be modeled by a coordination polyhedron which contains the transition metal and its electrons in their pure spin state in the glass host. Fitting observed spectra to a three-term empirical equation known as the spin-Hamiltonian for (for simple systems) allows the estimation of the crystal field splitting parameters and the relative covalency of certain bonds.[4,13,18]

F. Theory of Electron Spin Resonance [ESR]

It is necessary to understand some quantum mechanical concepts to grasp the fundamentals of ESR. The ensuing discussion attempts to summarize much of what has been described by Wong and Angell, and other researchers in the field.[13,18,19] The starting point is the resonance condition which was first discovered in 1945 by Zaroisky to observe the resonant absorption of Cu^{2+} with a frequency of 133 MHz and a magnetic field of 47.6 gauss. The resonance condition can be approximated as:

$$h\nu = g\beta H \qquad (2)$$

where h = Planck's constant, υ = frequency of radiation, g = Lande g factor β = the Bohr magneton, and H = magnetic field. It is helpful to examine the above condition and the effect on a free electron. The g factor is about 2.000 for a free electron, and the magnetic moment set up by the electron is contained in the Bohr magneton. A resonant absorption for this electron may be inferred from the above condition by 1) holding the frequency constant and altering (sweeping) the magnetic field until resonance is achieved i.e. $H = \frac{h\nu}{g\beta}$, or by 2) keeping H constant and varying the frequency $\nu = \frac{g\beta H}{h}$. The Cu^{2+} ion has an outer d^9 configuration 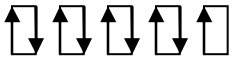 so the ion is in a paramagnetic state, and this was the basis for Zaroisky's findings.[18]

The resonance condition requires some further explanation, but only a simple discussion follows to promote general understanding of the technique. A free atom or ion may have a resultant magnetic moment [$\vec{G}$] (due to an unpaired spin) in its collection of electrons. The atom/ion will then have a permanent magnetic dipole moment denoted as [$\vec{\mu}$], and the two are equated by

$$\vec{\mu} = \gamma \vec{G} \qquad (3)$$

where γ is the magnetogyric ratio for the electron, which is constant and described by[18]

$$\gamma = -g\left(\frac{e}{2mc}\right) \qquad (4)$$

with e as the electronic charge, m is the electron mass, and c is the speed of light. The quantity referred to as the Lande factor [g] is a pure number whose value

depends on the relative contribution of orbital and spin to the total angular momentum.

The contributions of both orbital and spin angular momentum are important for determining where one will see resonances in an EPR spectrum. For a free electron, the g-factor is the ratio of the spin magnetic moment in Bohr magnetons to the spin angular momentum in units of h , with the value of 2.00 for the electron. The total orbital quantum number is denoted by L, and if only orbital momentum is present for the atom being probed, then $\vec{G} = \mathrm{h}\vec{L}$, with g = g_L which is 1.00. The total spin momentum quantum number is S, and if there is only electron spin momentum present, then $\vec{G} = \mathrm{h}\vec{S}$, with g = g_S which is 2.00 as per the free electron.

Quantum mechanics requires the use of mathematical operators that act on the various wave functions to yield measurable quantities. The orbital momentum operator is $\acute{\mathrm{L}}$, and spin momentum operator is denoted as $\hat{\mathrm{S}}$. If there are both orbital and spin angular momenta present, then the g value is a function of the coupling between these two, and the value will fall betweeen 1.00 and 2.00. In L-S coupling, the resultant angular momentum is associated with a new quantum number (operator) that is $\hat{\mathrm{J}}$, where $\hat{\mathrm{J}} = \acute{\mathrm{L}} + \hat{\mathrm{S}}$, so the resultant g value would assume the form of g_J. A benefit of studying solids with ESR is that the contributions of orbital momentum ($\acute{\mathrm{L}}$ operator) are quenched,[13] so that only the pure electron spin contribution which simplifies analysis.

There are additional considerations (none of which are intuitive) that together become the essence of the described resonance phenomena. In the presence of a magnetic field $\vec{H}$, the interaction between the electronic magnetic dipole moment and the field and the ensuing (Zeeman/split) energy levels are given by:

$$E = -\vec{\mu}_J \bullet \vec{H} = g_J \beta H M \qquad (5)$$

where M is the component of the electronic angular momentum $\vec{J}$ along the field acting on the atom. The magnetic dipole transitions are induced according to the

selection rule $\Delta M = \pm 1$, and when an alternating field of frequency υ is applied at right angles to $\vec{H}$, the result is that an energy quantum of $h\nu = g_J \beta H$ is absorbed so that the spin of the electron is flipped from a direction parallel to the magnetic field (lower energy level) to that of the anti-parallel direction (higher energy level).[18] The frequency range for the resonance absorption is typically X band (9-10 Ghz), with magnetic field values from 0 to 5000 Gauss employed for practical laboratory measurement. The relaxation time of the flipped spin must also be short for the paramagnetic states to be observed in ESR.

The obtained spectrum is specific for each species that might be probed. The scan of the magnetic field is on the horizontal axis, and absorption intensity is the vertical scale. Resonance absorptions are recorded by the instrumentation as in other spectroscopy methods and show up as peaks. However, to increase the signal to noise ratio, what is plotted and reported is the first derivative of each of the absorptions, as shown in Figure 10 for Fe^{3+}. The transition group ions with $3d^5$ configuration (Mn^{2+}, Fe^{3+}) have one electron in each d orbital, and by Hund's rule of maximum multiplicity, are in a singlet state S = 5/2. The free ion with this S-state also remains in the S=5/2 state when bound in a solid, a condition which is quite helpful to the analyst.

Because of the resonance phenomenon as described above, only certain categories of samples are fit for investigation. The required paramagnetism is seen in 1) atoms, molecules, and free radicals having an odd number of electrons (including atomic hydrogen, NO, and CH_3), 2) molecules with an even number of electrons which are not all spin-paired (O_2), 3) ions having partially filled inner electron shells such as transition and rare-earth metal groups, 4) metals and semiconductors containing conduction electrons. In addition, such electron paramagnetism can also be induced in solutions or solids by high energy particle or radiation bombardment, which give rise to color centers.

There are two primary methods for performing EPR experiments. The fundamental analysis attempts to describe the behavior of unpaired electrons of the free ion when placed in a solid environment. This procedure is inherently more difficult, and requires knowledge of the free ion spectra and characteristics,

and any perturbation the ion and its wavefunctions encounter in the presence of local electric fields established by neighboring ligands. One must then consider the various models of local 'crystal' environments, calculate the energy correction from the perturbation, and fit the calculated values to the observed parameters for splitting and hyperfine structure.

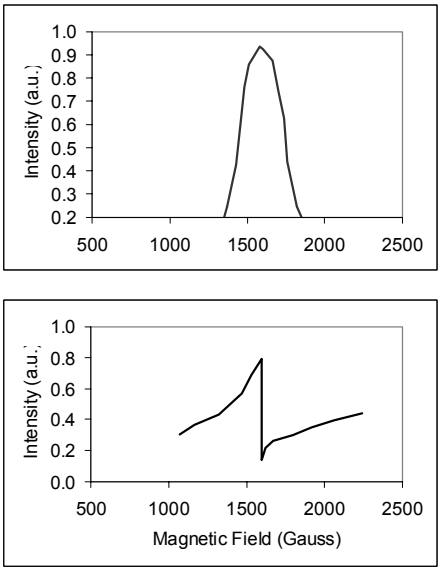

Figure 10. Representative (a) absorption and (b) first derivative ESR spectrum for Fe^{3+} in alkali-borosilicate glass. Absorption occurs at a magnetic field ≈ 1550 G at frequency ≈ 9.53 GHz, with average g ≈ 4.3

The second method is most used by spectroscopists and involves the formulation of the appropriate *spin Hamiltonian* to describe the experimentally observed parameters. There is an analogous spin Hamiltonian employed in nuclear magnetic resonance [NMR] spectroscopy. The spin Hamiltonian for ESR contains terms for the Zeeman interaction (splitting), hyperfine interactions, and second-order fine structure (or crystal field) interaction. The form for the effective axial spin Hamiltonian [$\boldsymbol{H}$][13,18] is

$$\boldsymbol{H} = \beta B \bullet g \bullet S + I \bullet A \bullet S + S \bullet D \bullet S \qquad (6)$$

where β is the Bohr magneton, B the magnetic field, S is the electronic spin vector, I the nuclear spin vector, and g, A, and D are matrices that describe the

energetics of the coupling between the magnetic fields associated with the electronic and nuclear vector quantities. It is important to note that matrices describe these values, and that there are orientational/directional differences that result—i.e. the specification of $g_{\perp}$ and g_{P} matrices for single crystals and polycrystalline samples depending on orientation with respect to the magnetic field. For glass samples, terms such as the g values may be averaged over the number of sites that contribute to the observed resonance [g_{eff}]. There are higher order correction terms in perturbation theory that are excluded because of the inability to measure their effects in glasses.

Despite the complex analysis, ESR remains a useful technique to detect even small amounts of paramagnetic ions in glasses. Unpaired spin concentrations as low as 10^{-12} may be detected, and amounts may be quantified with the appropriate 'spin standards'. The resonance features also quite sharp in oxide glasses, and spectra are highly reproducible for the species and host in question. ESR is also useful to determine the presence and concentrations of different oxidation states of transition metal ions.

II. EXPERIMENTAL METHOD

A. Batch Preparation

The present work required a glass that would soften at fairly low temperatures (≤ approximately 400° C), so the majority of the study concentrated on high B_2O_3-content glasses. Initially, an alkali borosilicate composition was chosen that contained large percentages of both B_2O_3 and SiO_2. The initial choice was 11.7 Na_2O•36.7 B_2O_3•51.6 SiO_2 (mol%). The batches of this type were formulated as 11.7 Na_2O•36.7 B_2O_3•(51.6-x) SiO_2•x MO, where MO represents the metal oxide. All compositions given in this study are in mol %. The batches for each type of glass were formulated from reagent-grade H_3BO_3, SiO_2, Na_2CO_3, (Alfa Aesar) and (Fisher). Transition metal dopants were incorporated via addition of the metal oxides or carbonates, i.e. reagent-grade Cr_2O_3, MnO_2, CuO, NiO, (Fisher), V_2O_5, Bi_2O_3, Mo_2O_3 (Aldrich), $MnCO_3$ (Fisher), $FeCO_3$ (Research Chemical Corp.), and Nb_2O_5 (H.G. Starck). This thesis only reports results for Cr, Mn, and Nb, as only these dopants exhibited luminescence upon excitation with long-UV/blue light.

Batches were melted in 90Pt•10Rh crucibles at 1350° C for between 2 and 3 hours. If the reduced oxidation state of an ion was desired (i.e. Mn^{2+}, V^{3+}, Cu^{+}), batches had activated charcoal added as the reducing agent in the amount of approximately 1 wt% of the batch. The reduced batches were melted in mullite crucibles for the same temperature and time. All glasses were poured into a steel mold and cast into bars. The doped-glass bars were annealed at 490° C for 1 hour, after which the furnace was shut off and allowed to cool slowly to room temperature. The compositions denoted 1-4 were all melted in 90 Pt•10 Rh crucibles at 1350° C for between 2 and 3 hours, and annealed for 1 hour at 450° C, after which the samples were cooled in the same manner. The reduced glasses were transparent, with no visible sign of residual carbon.

B. Absorbance Spectroscopy

For spectroscopy, thin slices of ≈ 2.5 mm were cut from each bar, and both sides were polished using 120, 240, 400, 600, 800, 1200 grit SiC papers. A

colloidal CeO_2 suspension was also used for final polishing. UV-Visible Specta were measrured on a Perkin-Elmer Lambda 900 to determine absorption which was normalized to absorbance by dividing by the sample thickness. Scans were performed from 300 to 800 nm, to determine the behavior of the doped glasses in the visible range of the spectrum.

C. Fluorescence Measurements

Photoluminescence behavior of the glasses was determined by the use of a SPEX Fluorolog 1680 0.22m double spectrometer with Spectracq software configured by Jobin Yvon Horiba, Inc. The samples were excited with 300, 366, and 450 nm light for emission acquisitions. The source was a 450 W Xenon Arc Bulb. Excitation acquisitions were performed by fixing the emission wavelength at the peak of the emission band and scanning for the peak excitation wavelength that gave the observed emission. Samples were also qualitatively observed with a model UVGL-58 Mineralight® Lamp that featured 254 and 366 nm UV radiation.

D. Differential Scanning Calorimetry

Differential Scanning Calorimetry [DSC] was performed to determine glass transition behavior up to 600° C. Measurements were made on a TA Instruments Q10 DSC in ambient atmosphere. A few mg of each glass were tested as very small chips in aluminum pans. The cell of the DSC was purged with a constant flow of N_2 gas at a rate of 50 mL/min. The DSC traces were normalized by dividing the heat flow data by the sample mass in mg.

E. Dilatometry

Linear coefficient of thermal expansion [CTE] for glass compositions was measured to match the thermal expansion of the GaN/InGaN materials. Data was recorded up to 600° C using a Dilatronic I LVDT double pushrod dilatometer with a silica reference material. The heating rate was 3.0 K/min.

F. Electron Spin Resonance [ESR] Measurements

ESR Measurements were performed on niobium-containing samples to determine if glasses contained Nb^{4+} along with Nb^{5+}. The instrument was a Varian E-Line Century Series ESR Spectrometer with a Varian E102 Microwave

Bridge. Scans were performed at room temperature (70° F or 21° C for all runs), at a fixed frequency of 9.531 GHz, and the magnetic field was varied from 0 to 5000 Gauss. The time constant was 0.10 s, and the measurement power was 120 mW.

III. RESULTS

A. Thermal Properties

1. Glass Transition

The initial choice of host glass composition centered on the alkali-borosilicate system. The starting point was a composition that contained significant fractions of both B_2O_3 and SiO_2. The idea was that the amount of silica could be reduced to lower the onset of glass transition, the amount of B_2O_3 could be increased to raise the coefficient of thermal expansion (from that of pure silica) as well as lower significantly the onset of glass transition (since vitreous B_2O_3 has $T_g \approx 250°$ C).

Four base compositions were studied, with the amount of B_2O_3 and SiO_2 being varied between each. The four compositions (in mol%) were: 1) 11.7 Na_2O•36.7 B_2O_3•51.6 SiO_2 2) 12 Na_2O•38 B_2O_3•50 SiO_2 3) 15 Na_2O•30 B_2O_3•55 SiO_2 and 4) 12 Na_2O•45 B_2O_3•43 SiO_2. All of the glasses were transparent, with no visible hint of crystallization or scattering due to phase separation. However, all compositions are known to fall within the region of spinodal phase separation for the alkali-borosilicate system. In addition, the glasses were non-durable as expected (because of the high B_2O_3 content) and developed surface corrosion products after a few weeks of storage at ambient conditions.

The DSC data indicate that all of the chosen compositions offer characteristics that are near to what is desired. In DSC, the onset of glass transition [T_g] is inferred by the intersection of a line from the horizontal baseline with the a line from the inflection point of the endotherm. The DSC data for glasses 1, 2, and 4 are represented in Figure 11, and Figure 12 shows the DSC trace for composition 3.

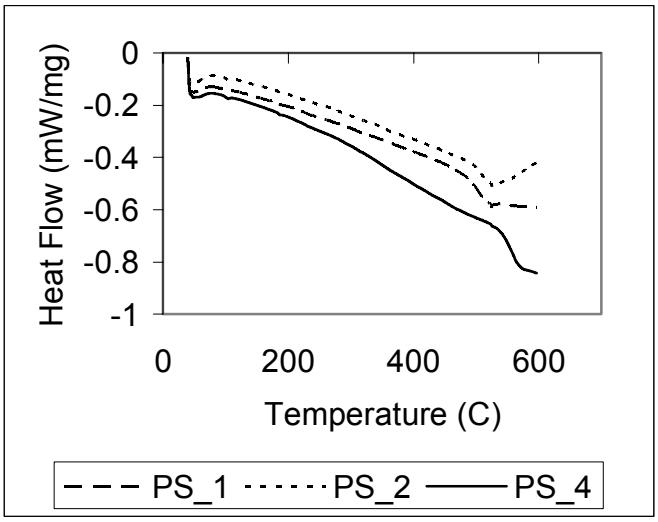

Figure 11. DSC data for Compositions 1, 2, and 4.

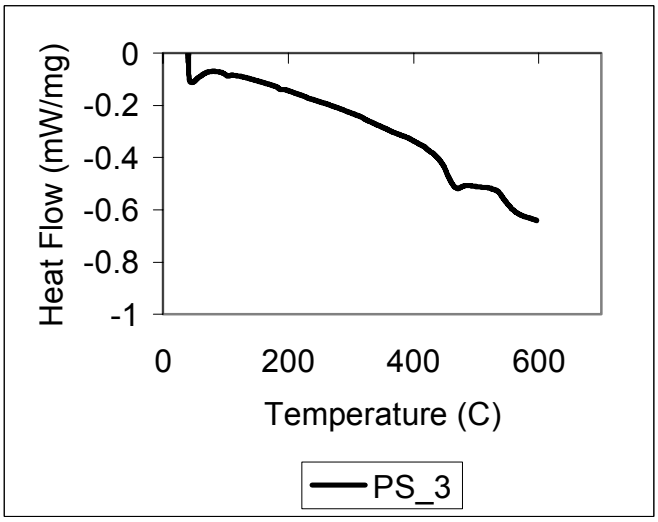

Figure 12. DSC data for Composition 3.

2. Linear Thermal Expansion

Thermal expansion may be customized for a particular glass application via compositional changes. The dilatometric softening point [T_d] may also be found from the expansion curves, which gives an indication of the softening range of the glasses. There is variation in the obtained values for linear coefficient of thermal expansion [CTE], which is demonstrated in Figure 13. Expansion data has been plotted from about 50 to 600° C. The expansion behavior of the glass in the region from about 100 to 400° C is deemed important for the intended

phosphor system, and all samples show a fairly constant CTE in this temperature interval. The dilatometric softening point is resolved well only for compositions (2) and (3), and are approximately 550° C and 500° C, respectively.

The thermal expansion of GaN, InGaN, and SiC LED materials is quite low, ranging from 2-4 ppm*K^{-1}, 1-5 ppm*K^{-1}, and 2-4 ppm*K^{-1}, respectively. The thermal property data for the glasses studied are given in Table 3. The CTE observed for compositions (1) and (2) match these ranges quite well. The CTE of (3) and (4) are up to 3 times as high as the ranges given for the GaN materials, but this is not an unreasonable mismatch—particularly if one were interested in the application of a sintered glass coating.

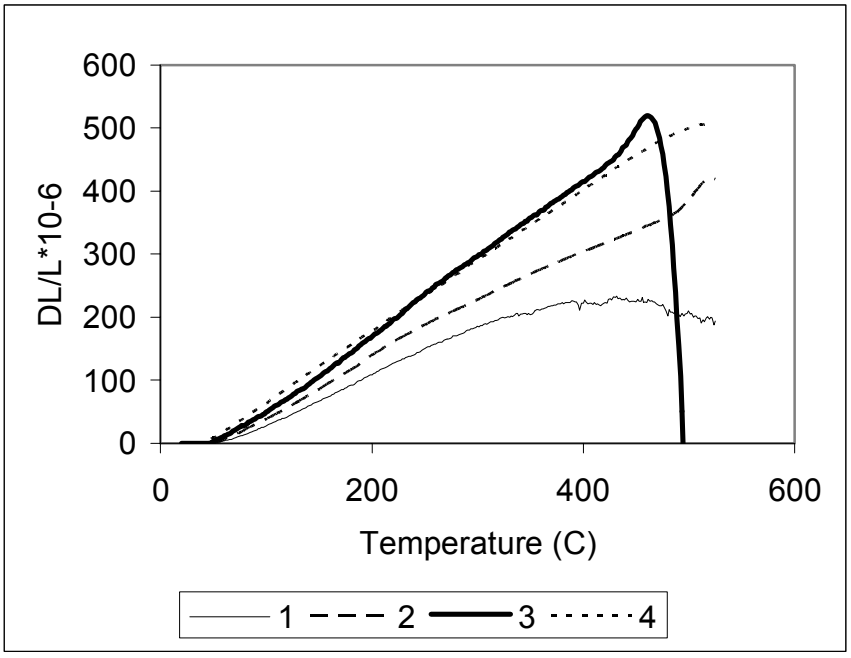

Figure 13. Linear thermal expansion data for Compositions 1-4. The expansion of each glass is seen to be fairly constant from about 100 to 400° C, though (1) experiences some softening at about 400° C. A distinct T_d is not seen for composition (1), however.

Table III. Summary of Thermal Data. Expansion data is between 50 and 400° C, except for 1) which is from 100 to 400° C.

Glass Composition	Onset of Glass Transition [T_g] (° C)	Dilatometric Softening Point [T_d] (° C)	Coefficient of Thermal Expansion (*10^{-6} K^{-1})
1) 11.7 Na_2O•36.7 B_2O_3•51.6 SiO_2	≈ 490	--	≈ 3.0
2) 12 Na_2O•38 B_2O_3•50 SiO_2	≈ 502	≈ 550	≈ 5.0
3) 15 Na_2O•30 B_2O_3•55 SiO_2	≈ 440	≈ 500	≈ 13
4) 12 Na_2O•45 B_2O_3•43 SiO_2	≈ 547	--	≈ 12

B. Spectroscopic Measurements

The most relevant spectroscopic results for Cr, Mn, and Nb are presented here, since these are the dopant ions that would be most useful for the intended frequency-shifting purpose. In this study, luminescence was seen in Cu^+, W^{4+}, and Sn^{2+} upon excitation with 254 nm UV light, but the short wave excitation energy is not applicable to the desired phosphor. The results for these and non-luminescent transition metal ions have not been reported.

1. Chromium Absorption and Luminescence

Initial investigation of the Cr^{3+} ion in the glass showed a very broad but weak fluorescent emission upon excitation with 450 nm light. The absorbance spectrum shown in Figure 14 is indicative of octahedral Cr^{3+} with well-known absorptions indicating the green color of the glass; there is an absorption minimum around 550 nm.

Some of the electronic structure may be calculated from the abosrbance spectrum. As shown in Figure 15, there are 3 broad peaks corresponding to the υ_1, υ_2, and υ_3 transitions with maxima at approximately 624 nm for υ_1, 432 nm for υ_2, and 340 nm for υ_3. No shift in the peak maximum is evident for the different concentrations. The absorption peaks correspond to the $^4A_{2g}$-->$^4T_{2g}$ for υ_1, $^4A_{2g}$ -->$^4T_{1g}$ (F) for υ_2, and $^4A_{2g}$-->$^4T_{1g}$ (P) for υ_3. The υ_3 transition allows the value of 10Dq to be calculated directly from the absorption peak maximum at 624 nm (≈ 16,025 cm^{-1}), and calculation of the Racah parameter B.[4] The method is shown in

Table IV, with relevant comparison data. The value of B gives an indication of the degree of covalent bonding present between the central ion and its ligands.[4,8,9] B' is calculated from

$$15B = \upsilon_3 + \upsilon_2 - 3\upsilon_1 \quad (7)$$

The calculated value for B' is ≈ 300 cm^{-1} which is very low, and does not correspond very well with the expected value in silicate or other glasses.[4,10,11,14]

The fluorescence spectrum corresponds to that of Cr^{3+} in a distorted octahedral site and is shown in Figure 15. There is a very low intensity emission in the near IR region upon excitation with 450 nm light, which corresponds to the $^2E \rightarrow {}^4A_2$ transition. The $^4T_1$ and $^4T_2$ states decay non radiatively (via heat) to the metastable state ^2E. The highest intensity occurs with 0.01 mol% Cr_2O_3 addition, and the fluorescence is rapidly quenched with increased Cr_2O_3 content. It should also be noted that the there was no visible luminescence in the samples upon excitation with the Mineralight® lamp.

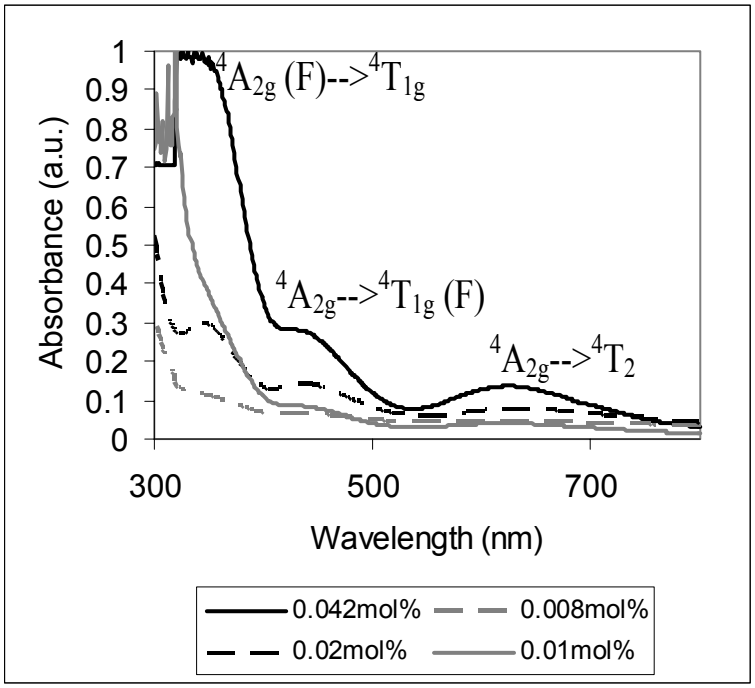

Figure 14. Absorbance spectrum for 11.7 Na_2O•36.7 B_2O_3•(51.6-X) SiO_2•X Cr_2O_3 glass. The X concentrations are shown in the legend.

Table IV. Calculation of Splitting Parameters for Cr^{3+} in above glass. Method adapted from A. Paul.[4]

Energy Level	Transition	Predicted Energy	Observed Energy (cm^{-1}) from Fig. 2.1	Energy for $(CrF_6)^{3-}$ From ([4])
↑	$^4T_{1g}(P)$	12Dq+15B+X	29,400	34,400
↑	$^4T_{1g}(F)$	18Dq - X	23,150	22,700
↑	$^4T_{2g}$	10Dq	16,025	14,900
	$^4A_{2g}$	0		
υ_1 υ_2 υ_3			Dq ≈ 1,600 cm^{-1}	1490 cm^{-1}
			B ≈ 300 cm^{-1}	827 cm^{-1}

Note: $X = (225B^2 + 180B \bullet Dq + 100Dq^2)$

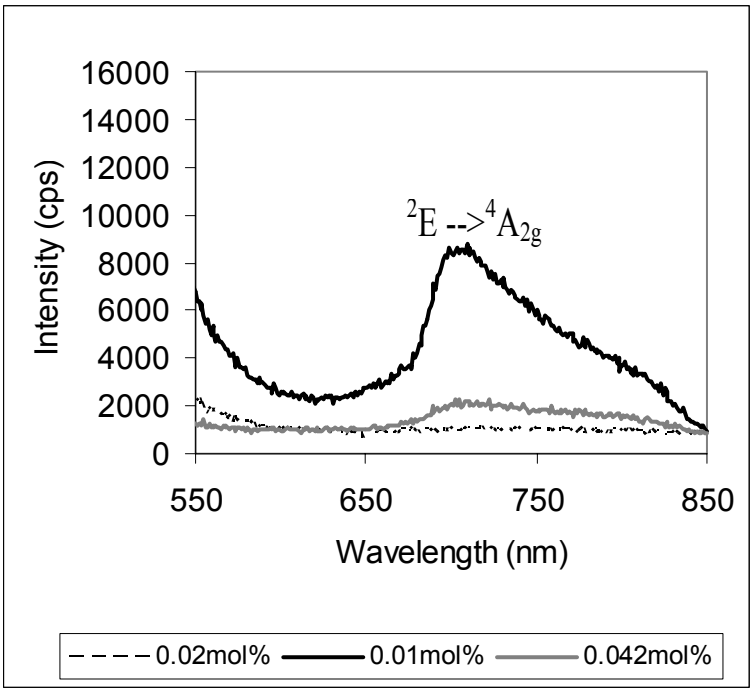

Figure 15. Fluorescence spectrum for 11.7 $Na_2O \bullet 36.7\ B_2O_3 \bullet (51.6\text{-}X)\ SiO_2 \bullet X\ Cr_2O_3$ glass. Excitation was at 450 nm.

2. Absorption and Luminescence of Manganese

The manganese-doped glasses were very different in appearance, depending on the redox conditions. Batches that were not reduced were dark purple. A mix of oxidation states remained in the reduced batches. Inhomogeneities in the reduced glasses were indicated by the presence of small

amounts of Mn^{3+} (as purple swirls) intermixed with the remaining clear/yellow glass. The absorbance spectrum for 11.7 Na_2O•36.7 B_2O_3•(51.6 –x) SiO_2•x MnO Glass (mol%) is shown in Figure 16. There is a very strong absorption located at approximately 410 nm, corresponding to the ^6S-->$^4A_{1g}$, ^4E (G) transition.[3,4,12] The fluorescence spectrum in shown in Figure 17. The large excitation peak with a maximum at 410 nm corresponds directly to the ^6S-->$^4A_{1g}$, ^4E (G) shoulder at the same wavelength in the absorbance spectrum. The 0.45 mol% MnO glass has its maximum shifted down to about 408 nm. In excitation, one can also note the following: the $^6A_{1g}$ (^6S)-->^4E_g (^4D) transition at roughly 345 nm, with a shoulder at 360 nm corresponding to the $^6A_{1g}$ (^6S)-->$^4T_{2g}$ (^4G) transition. There is also a broad and intense excitation peak with a maximum at around 505 nm, corresponding to the $^6A_{1g}$ (^6S)-->$^4T_{1g}$ (^4G) transition. The very broad and intense orange fluorescent emission is made up of two transitions to the ground state: the $^4T_{1g}$-->$^6A_{1g}$ (^6S) transition at roughly 600 nm, and the $^4T_{2g}$-->$^6A_{1g}$ (^6S) transition at about 650 nm.

It is possible to calculate some of the structural parameters for the manganese-doped glasses from the excitation spectrum. No sharp bands other than ^6S-->$^4A_{1g}$, ^4E can be resolved in the absorbance spectrum for Mn^{2+}. The Racah parameters B and C may be calculated from the peak positions of the two ^4E excited bands in Figure 17. The two ^4E levels are constant regardless of the field strength, which may be seen in Figure 8, and the difference between these two levels is equal to 7B.[3,4,12] The energies of the two ^4E levels have been resolved, and are given by the sharp peaks at approximately 345 nm (28,990 cm^{-1}) and 410 nm (24,390 cm^{-1}), which correspond to the known absorbances of Mn^{2+} in various crystals, glasses, and in solution.[3,4,12] The quantity 7B is equal to the difference between the ^4E levels given above, so

$$7B = {}^4E_{high} - {}^4E_{low} \quad (8)$$

$$B = (28{,}990 - 24{,}390)\ cm^{-1} \quad (9)$$

$$B \approx 660\ cm^{-1} \quad (10)$$

Knowing B allows calculation of the Racah parameter C from the specified energy equations or matrices for the transitions.[6] The energy difference between the ^6S ground state and the $^4A_1$ (^4G) state (which is degenerate with the lower ^4E level and also constant) is given by[6,12]

$$10B + 5C = \text{Energy of } {}^4A_1 ({}^4G) \tag{11}$$

Using the value of 24,390 cm^{-1} for the energy, and $B \approx 660$ cm^{-1}, we have:

$$10*(660) + 5C = 24{,}390 \text{ cm}^{-1} \tag{12}$$

$$C \approx 3500 \text{ cm}^{-1} \tag{13}$$

The values calculated for B and C for Mn^{2+} in the glass are in accordance with the work of others,[8,9,12] so the estimation of the parameters is reasonable. Results are summarized in Table V. The B value is shifted lower than that of the free ion (860 cm^{-1}) as given in Table II.

The value of Dq for the Mn^{2+}/O^{2-} in the studied glass would indicate the field strength of the combination, but requires higher resolution methods than have been available. The energy matrices for the various bands have been specified by Orgel in the weak-field approximation,[3] and Tanabe and Sugano for low to high fields.[6] The calculation of Dq from the above matrices is only possible if the peak positions of the higher energy excited bands can be closely determined. The current fluorimeter offers almost no resolution for wavelengths below 300 nm, and none of the bands on the high energy side are seen in absorbance. Measurements of % transmittance are often used to find small-magnitude deviations from the baseline (absorptions) throughout the UV/Visible range, but such tests did not resolve any of the higher energy bands of the absorption spectrum in this work.

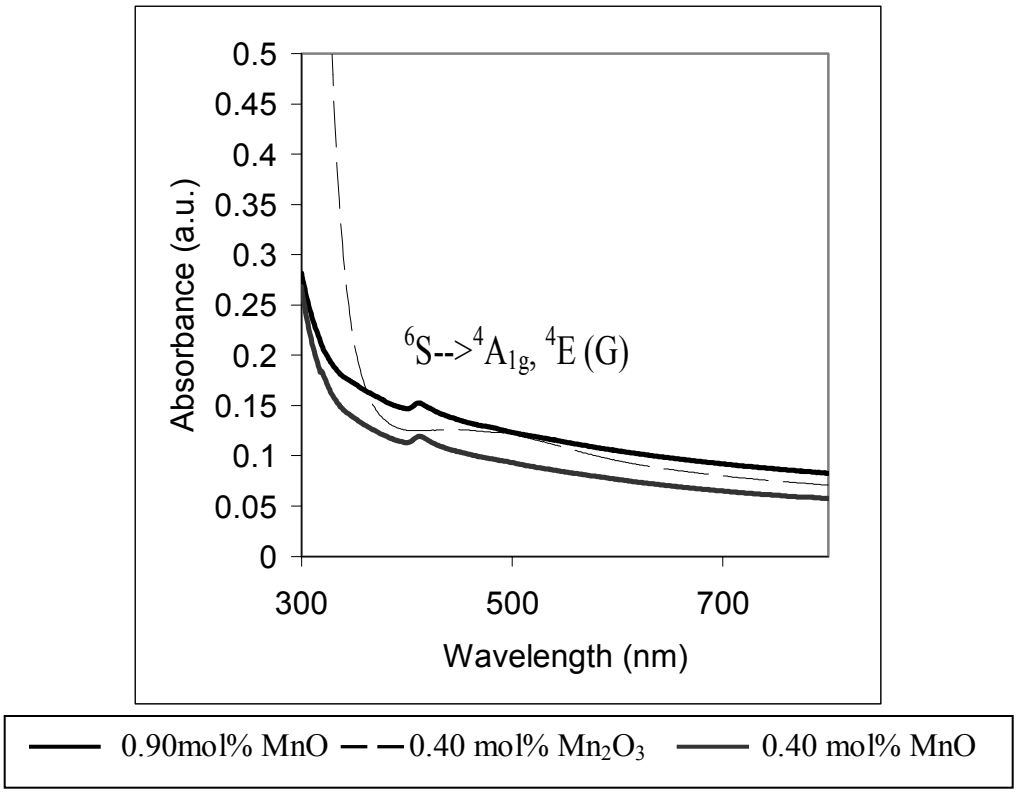

Figure 16. Absorbance spectrum for 11.7 Na_2O•36.7 B_2O_3•(51.6-X) SiO_2•X MnO/Mn_2O_3 glass. The indicated absorption transition is evident at around 410 nm for the reduced samples.

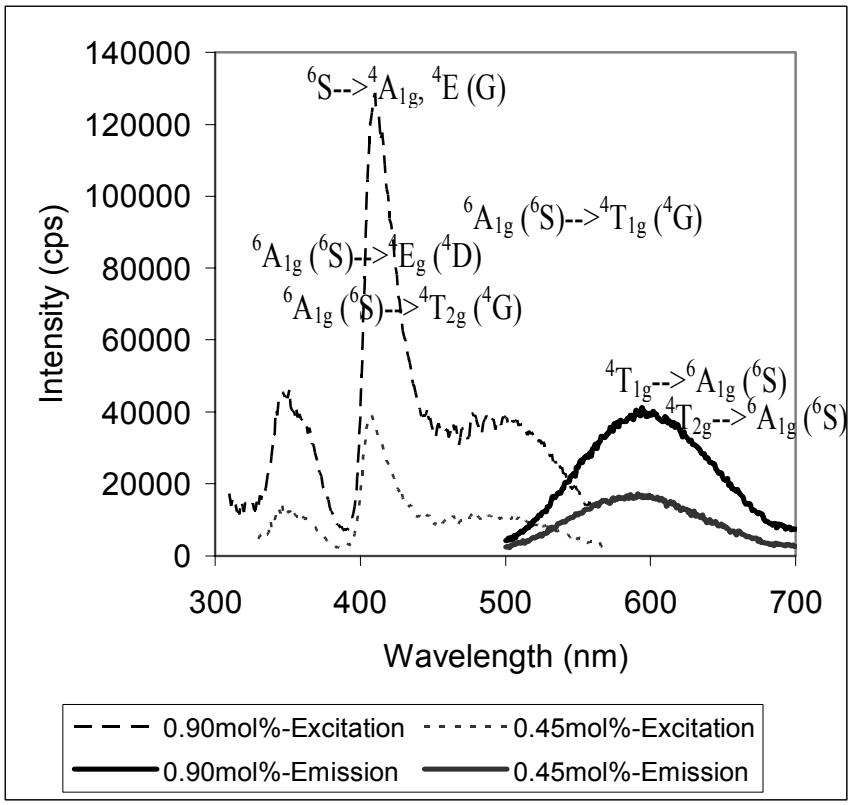

Figure 17. Excitation (emission 600 nm) and emission (excitation 450 nm) Spectra for 11.7 Na_2O•36.7 B_2O_3•(51.6-x) SiO_2•x MnO glass. The excitations at roughly 354 and 505 nm are responsible for the luminescence at roughly 600 and 650 nm, which result in the very broad emission.

Table V. Summary of Transition Data for Mn^{2+}.

Transition ^6S-->	Observed Energy (cm^{-1}) from Fig	Wavelength (nm)	Energy in (cm^{-1}) for Na_2O•4B_2O_3:5MnO (mol%)[12]
$^4T_{1g}$ (^4G)	19,800	≈ 505	19,300
$^4A_{1g}$, ^4E (G)	24,390	≈ 410	24,430
$^4T_{2g}$ (^4G)	27,780	≈ 360	-
^4E (^4D)	28,990	≈ 345	28,700
	B ≈ 660 cm^{-1}		B ≈ 630 cm^{-1}
	C ≈ 3500 cm^{-1}		C ≈ 3610 cm^{-1}

3. Absorbance and Emission of Reduced Niobium Glass

The absorbance spectrum for reduced 11.7 Na_2O•36.7 B_2O_3•51.5 SiO_2•0.1 Nb_2O_5 glass (mol%) is shown in Figure 18. The glass was clear and colorless, and there were no strong absorptions resolved by the UV/Visible measurements within the instrument parameters. The emission spectrum (excitation at ≈ 366 nm) is shown in Figure 19, and the excitation spectrum (emission at 605 nm) is given in Figure 20. The emission spectrum shows a broad band at roughly 450-500 nm (blue-green), and an orange emission centered at about 605 nm. Both of these luminescence transitions are of high intensity. It is also of interest that the glass displayed two different fluorescence colors upon excitation with the Mineralight. The 254 nm radiation caused a yellowish-white fluorescence, while the 366 nm UV caused the samples to emit an orange color.

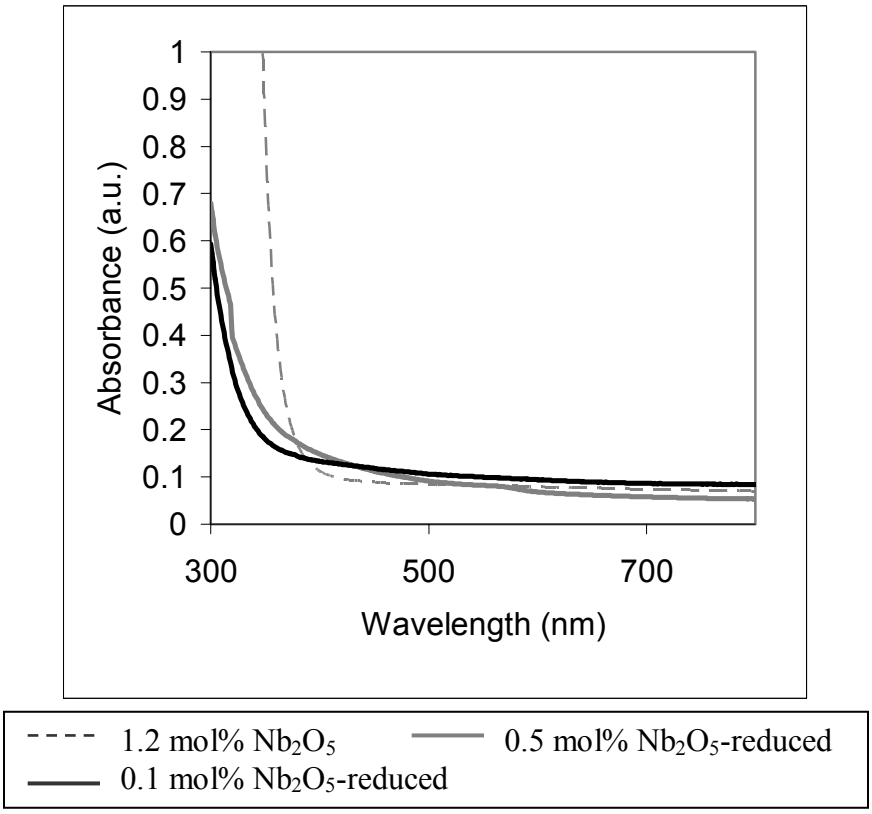

Figure 18. Absorbance spectrum for 11.7 Na_2O•36.7 B_2O_3•(51.6-x) SiO_2•x Nb_2O_5 glasses. No specific absorption peaks are evident.

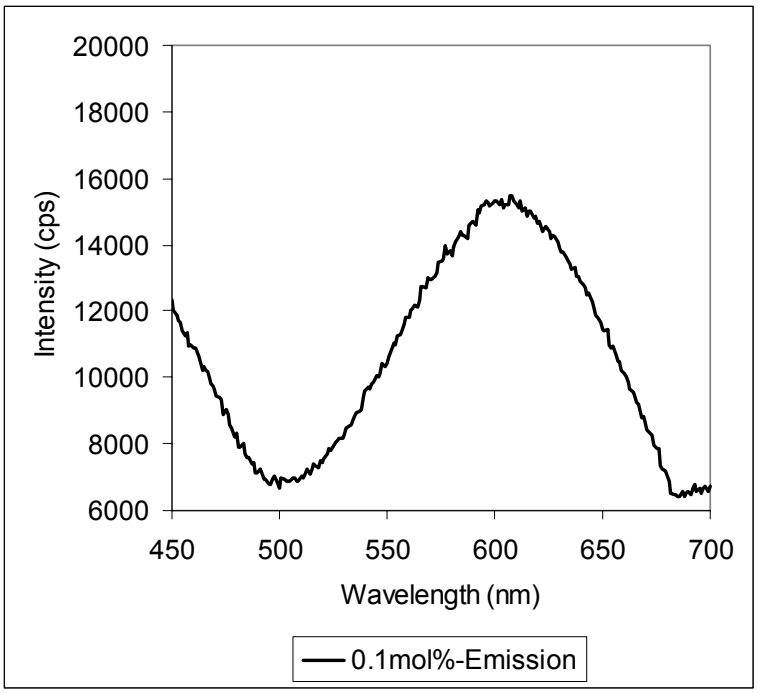

Figure 19. Emission spectrum (exciation 366 nm) for reduced 11.7 Na_2O•36.7 B_2O_3•51.5 SiO_2•0.1 Nb_2O_5 glass. There is a high intensity and broad-band orange emission centered at about 605 nm, and additional broad blue emission intensity is seen on the low wavelength side.

Fluorescence in niobate crystals has been studied by numerous researchers.[1,20-22] Additionally, luminescence in niobium-containing glasses has also been reported in the work of others.[16] In crystals, Nb^{5+} generally attains octahedral coordination. NbO_6 octahedra are responsible for most of the reported luminescence phenomena, however NbO_6 displays efficient luminescence only when niobyl groups (Nb—O) are present that feature a short bond distance of approximately 0.17 nm. This conclusion is supported by the observation that some of the ordered niobate perovskites, such as $MgNb_2(P_2O_7)_3$ do not display efficient luminescence, but distorted niobate structures may show efficient luminescence.[16] An example of such a distorted niobate group would be $LaNbO_4$, in which the Nb^{5+} attains a 4 + 2 coordination, which causes the appearance of the distorted niobyl groups and the observed luminescent transitions. In addition it is said that edge or face-shared NbO_6 octahedra show efficient absorption and luminescence, while corner-sharing of NbO_6 leads to a shift in optical absorption

(to lower energies) which results in energy migration and subsequent quenching of the luminescence.[16]

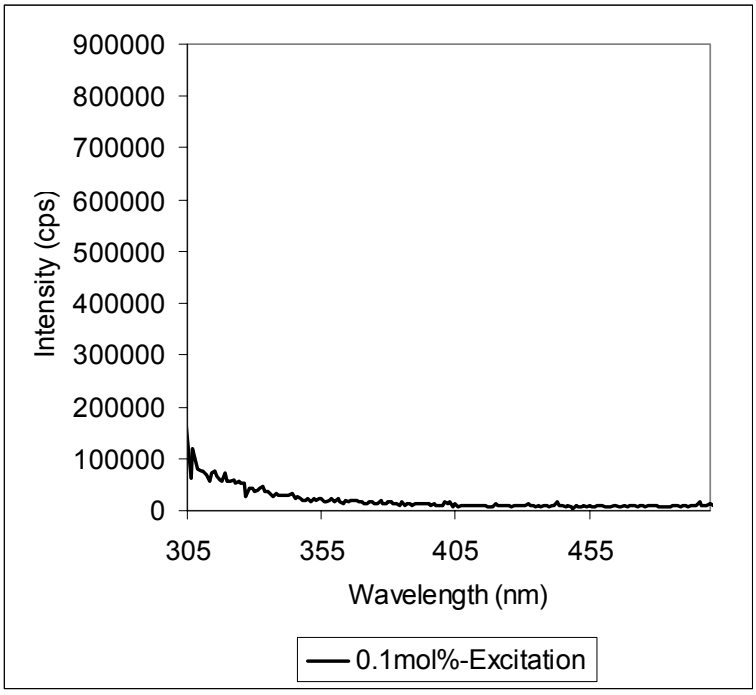

Figure 20. Excitation spectrum of reduced 11.7 Na_2O•36.7 B_2O_3•51.5 SiO_2•0.1 Nb_2O_5 glass. There are no resolved absorption peaks, as for Mn^{2+} but there is a significant band of UV absorption at $\lambda \leq 375$ nm.

A similar model has been developed for the V^{4+} ion in glasses.[23,24] Vanadium lies directly above niobium in the periodic table, so the outer electronic configurations of Nb^{4+} and V^{4+} are the same. Vanadium exists in various glasses within tetragonally-distorted octahedra. The tetragonal distortion is due to the vanadyl (VO^{2+}) ion which displays a shortened bond distance in relation to the vanadium ion with the other oxygen ligands. The presence of this structure has been studied by ESR, and interpreted in terms of the molecular orbital description of Ballhausen.[2,23] The Nb^{4+}-containing $(NbO_6)^{8-}$ octahedra likely correspond to the same type of model within glasses. The reason for the luminescence properties of the Nb^{4+}-containing glasses is not clear in terms of the above model.

It is evident that glass systems, with their short-range order, could create some of the distorted niobate structures that seem to be required for photoluminescence. In this work, only the reduced niobium-containing glasses showed any type of fluorescence, and only at low percentages of Nb_2O_5 addition. The oxidized melts did not visibly luminesce in either the fluorimeter or upon excitation with the Mineralight®. Based upon previous studies in crystals, the Nb^{5+} ion is responsible for the observed fluorescence, and not a reduced state of niobium (i.e. Nb^{3+} or some other state) however, the presence of other oxidation states of niobium facilitates distortion of the Nb^{5+} sites. It may be possible to achieve luminescence in oxidized niobium-containing glasses with very low percentages of dopant, provided that the glass structure can be made to sufficiently distort the NbO_6 octahedra. However, the absorption and luminescence properties of the niobium-containing glasses are not well known at this time.

4. ESR Measurements on Niobium Glasses

The presence of Nb^{4+} ions in the glass may be determined from ESR measurements. The Nb^{5+} ion is thought to be more common in glasses, and possibly act as a glass former in higher amounts. Nb has the electronic configuration [Kr] $5s^2$ $4d^3$. The Nb^{5+} ion would then assume the [Kr] configuration, for which all shells are filled with paired electrons, and the resulting ion is diamagnetic. The Nb^{3+} ion could 1) have its two 5s electrons and one 4d electron removed leaving [Kr] $4d^2$ which is diamagnetic, or 2) have all $4d^3$ electrons removed, leaving [Kr] $5s^2$, which is also a diamagnetic situation. The Nb^{4+} ion has the three 4d electrons removed and one in 5s, leaving [Kr] $5s^1$, which is a paramagnetic ion. The unpaired electron in Nb^{4+} should absorb microwave radiation according to the resonance condition alluded to earlier for electron spin resonance, and so even small amounts of Nb^{4+} ion should be detectable through the use of ESR. The primary interaction of the unpaired electron is with field due to the six O^{2-} ligands (all diamagnetic), and with the ^{93}Nb nucleus (with I = 9/2, 100% abundance).[25] The O^{2-} ligands will have little effect on the observed resonance absorption spectrum, but the proximity of ^{93}Nb

nuclei to the absorbing electron should cause hyperfine splitting of the energy levels, resulting in 10 lines (# Lines = 2I + 1) of hyperfine splitting that should be observed. Additionally, the g values for the resonance will not be equal to 2.00 as for the free electron. The ^{93}Nb nucleus will contribute orbital angular momentum such that the observed g values will be shifted to values less than 2.00 (g = 1.00 is the g value for pure orbital momentum contribution).

ESR measurements were performed in a qualitative manner. The author found only one comprehensive study concerning the detection of Nb^{4+} in glasses, which was performed by Kim, Reardon and Bray.[26] The work of Kim et al. was centered on finding Nb^{4+} ions as a gamma-irradiation induced defect. The ESR spectrum of H.C. Starck Nb_2O_5 powder is given in Figure 21.

Glasses that contain Fe^{3+} display sharp and well-documented features in ESR spectra. The Fe^{3+} resonance occurs at average $g \approx 4.3$, which has been seen in a number of studies, and is shown in Figure 22 for Corning 7070 lithium/potassium borosilicate doped with 2.0 weight% Fe_2O_3 (courtesy of D. Rapp).

The niobium-containing glasses also display the presence of iron, but are the spectra are quite different on the high field side of the scan. Figure 23 shows the ESR spectrum for the oxidized 11.7 Na_2O•36.7 B_2O_3•50.5 SiO_2•1.2 Nb_2O_5 glass. The presence of Fe^{3+} is evident which is due to contamination from the batch materials. The same situation is seen in Figure 24 for the reduced 11.7 Na_2O•36.7 B_2O_3•51.5 SiO_2•0.1 Nb_2O_5 glass. The amount of Fe^{3+} appears to be less, due to the reduction of ferric to ferrous iron. The reduced niobium glass displays a multiple resonance feature which is due to the hyperfine splitting interaction of the lone Nb^{4+} 5s electron with the ^{93}Nb nucleus. This feature is not present in the spectrum of the oxidized sample of Figure 23, though it is weakly resolved in the Nb_2O_5 powder spectrum—indicating a slight degree of non-stoichiometry. It is possible that Nb^{3+} is present in the reduced glass or powder, but it would not be detected in ESR since it is not paramagnetic.

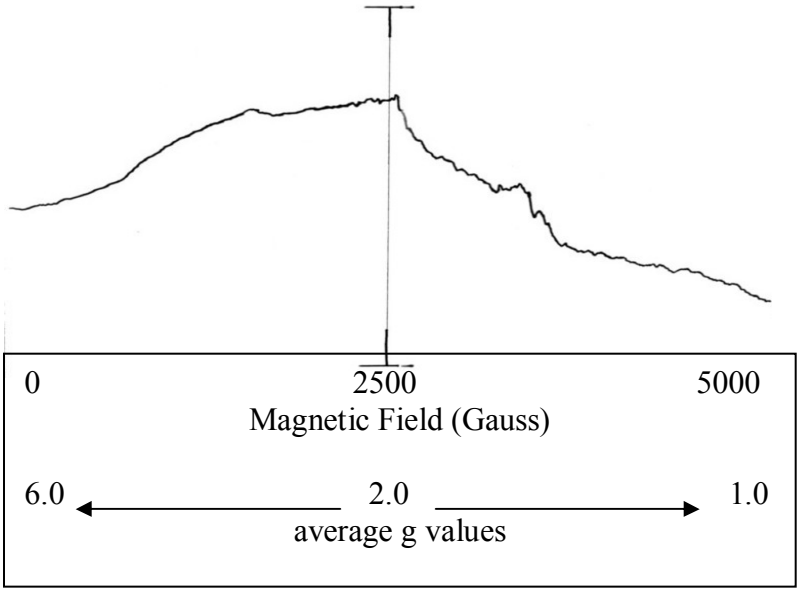

Figure 21. First derivative ESR spectrum of H.C. Starck Nb_2O_5 powder. The lack of any resonance features for Fe^{3+} indicates high purity. There is also indication of multiple resonances at $g \approx 1.90$ which is in the middle of the expected Nb^{4+} spectrum..

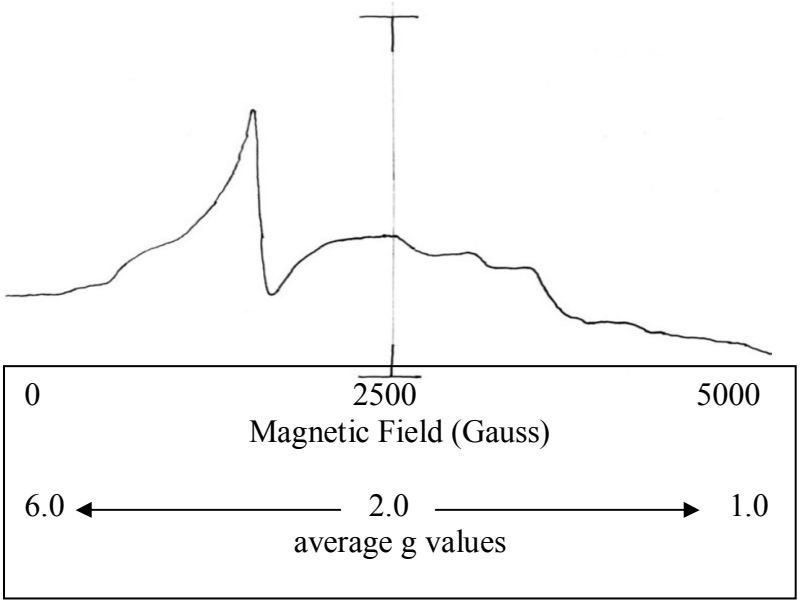

Figure 22. Corning 7070 glass doped with 2.0 wt% Fe_2O_3 (courtesy of D. Rapp). The Fe^{3+} resonance is well-resolved, with $g \approx 4.3$

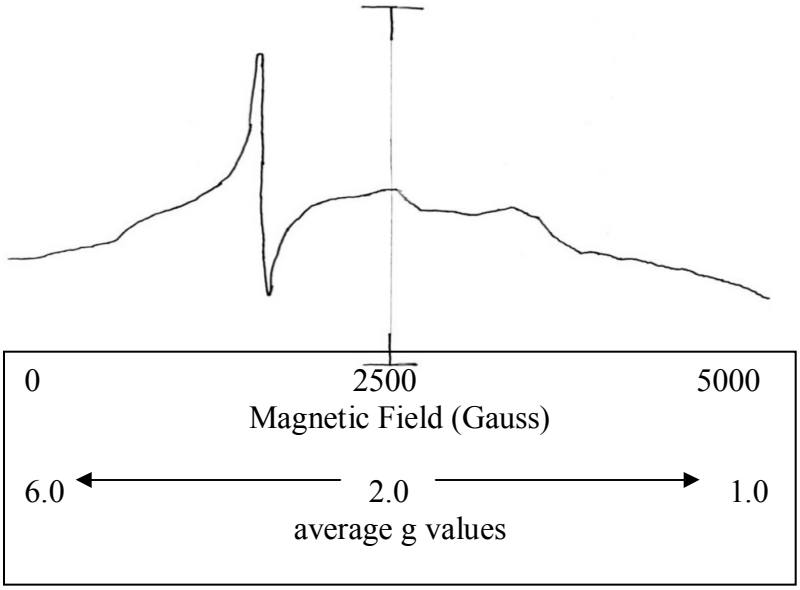

Figure 23. ESR spectrum for 11.7 Na_2O•36.7 B_2O_3•50.5 SiO_2•1.2 Nb_2O_5 glass. The presence of Fe^{3+} is most likely due to raw materials. The high magnetic field side of the sweep does not display any hyperfine splitting due to ^{93}Nb.

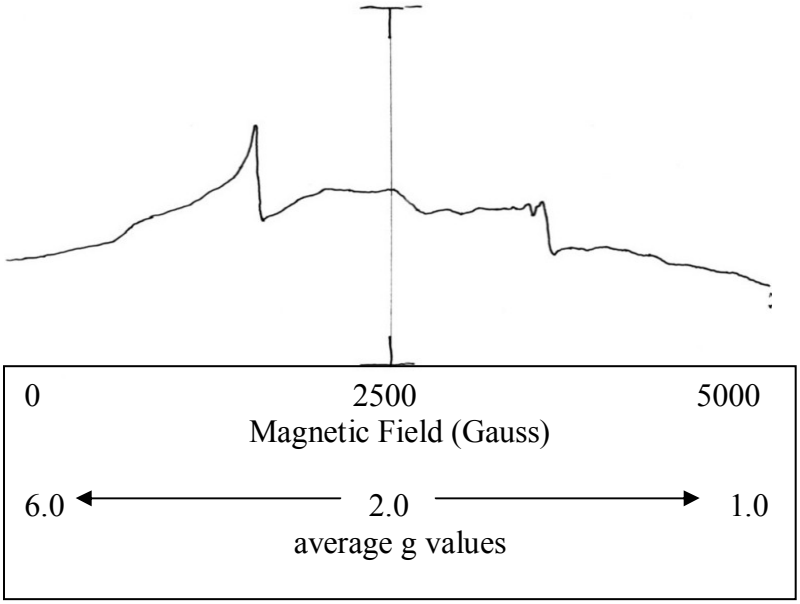

Figure 24. ESR spectrum for reduced 11.7 Na_2O•36.7 B_2O_3•51.5 SiO_2•0.1 Nb_2O_5 glass. The resonance due to Fe^{3+} contamination is again visible at $g \approx 4.3$, but one may also note the multiple resonance feature that occurs at $g \approx 1.9$. This corresponds directly to the middle part of the broad spectrum observed by Kim et. al.[26]

The ESR technique offers high sensitivity but use of the manual chart recorder did not enable resolution of all hyperfine splitting resonances. Kim, Reardon, and Bray were able to simulate a spectrum with a computer that matched the experimental, and which clearly resolved all ten lines.[26] The spectrum shown in Figure 24 captures the strongest resonances, which are likely the electronic levels due to the I = 3/2 and I = 1/2 nuclear interaction. The resonances due to the higher I values -9/2, -7/2, and 7/2, 9/2 are resolved on the low and high field sides of the strongest resonances (I = 3/2, 1/2) respectively in the spectrum of Kim, Reardon, and Bray, but are of low intensity.[26] The same situation was evident in this study, but the presence of the hyperfine levels described indicates the presence of the paramagnetic Nb^{4+} ion.

5. Co-Doped Glass—Manganese and Niobium

An attempt was made to combine the luminescence of Mn^{2+} and $Nb^{4+/5+}$ by co-doping in the same glass. The batch was heavily-reduced as described in section II, and the desired composition was 11.7 Na_2O•36.7 B_2O_3•50.6 SiO_2•0.9 MnO•0.1 Nb_2O_5. The resulting glass was dark purple, due to the presence of significant Mn^{3+}, which means that it is more likely that two Mn are associated with three oxygens, so that the desired composition was not achieved. The sample emitted orange light of weak intensity under excitation by both 254 and 366 nm UV light from the Mineralight®. The excitation and emission spectrum is shown in Figure 25. The excitation and emission intensities have been reduced in comparison to the singly-doped 0.9 mol% MnO glass because of the lesser concentration of Mn^{2+} (and subsequently large amounts of Mn^{3+}) and the absorption of orange/red light by Mn^{3+}. The peak emission has also been red-shifted to about 610 nm (16,393 cm^{-1}).

The emission spectrum of the co-doped glass shows some evidence of the short-wave UV fluorescence described in Section 3. There appears to be low intensity 'tail' on the low-wavelength side of emission which is similar to that seen in the emission spectrum of Figure 19. The curve is seen to reach its peak on the low wavelength side of the spectrum at about 400 nm (cm^{-1}), after which the

intensity decreases again. This emission band probably corresponds to part of the visible greenish-white fluorescent color under 254 nm UV excitation.

ESR measurements were also performed to detect Nb^{4+} in the co-doped glass. Mn^{2+} is known to exhibit strong resonances in ESR at $g_{eff} \approx 2.0$. The Mn^{2+} signal overwhelmed any predicted spectral features. The Mn^{2+} resonance was of high intensity and was off the scale of the manual chart recorder. The result was that the expected signal due to Nb^{4+} was not seen. Attempts at dilution of the samples also did not yield satisfactory results.

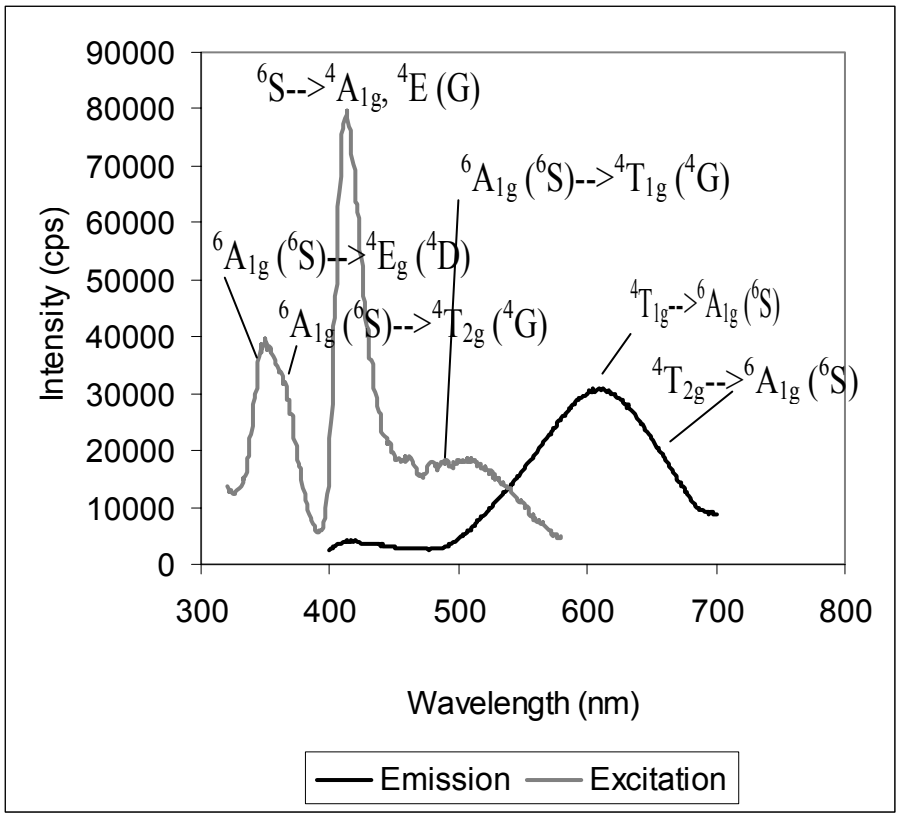

Figure 25. Excitation (emission 610 nm) and emission (excitation 366 nm) spectrum of reduced 11.7 Na_2O•36.7 B_2O_3•50.6 SiO_2•0.9 MnO•0.1 Nb_2O_5. All of the excitation peaks correspond to Mn^{2+}. There is also evidence of significant UV absorption below ≈ 320 nm. The peak emission has been shifted to ≈ 610 nm. Excitation and emission intensities are of much lower intensity than for singly-doped Mn^{2+} glass

IV. DISCUSSION

A. Transition Metal Sites in Alkali-borosilicate Glass

The glass compositions studied lie in the phase separation region for the ternary $Na_2O•B_2O_3•SiO_2$ system.[27,28] Phase separation was not visible to the eye after preparation of the samples. Atomic force microscopy [AFM] has proven to be a powerful technique for studying details of phase separation on the order of tens on nanometers (Wheaton and Clare, 2004), but observations with AFM did not show a separated morphology for any of the compositions studied.

Glasses in the $Na_2O•B_2O_3•SiO_2$ system exhibit several mechanisms of phase separation as well as an asymmetric immiscibility dome, depending on the amounts of the glass formers B_2O_3 and SiO_2.[28] Compositions similar to those studied exhibit spinodal decomposition even upon cooling, which is the likely scenario in this investigation. The phases present are a high silica phase (roughly 96% homogeneous), and an $Na_2O•B_2O_3$ phase.[28] The silica phase contains very few non-bridging oxygens [NBO], and rejects the introduction of the transition metal ions, so they move preferentially into the sodium borate phase. The interconnected morphology implies that the sodium borate phase and TM ions contained within are well-dispersed throughout any particular glass sample. The dimension of such spinodally-phase separated features is on the order of tens of Angstroms,[28] which is the reason these features have not been resolved in AFM.

The role of the TM ions in the sodium borate phase is similar to that of alkali in the melt. The TM ions occupy positions in the melt upon cooling as would the smaller alkali, and induce the conversion of BO_3 triangles to BO_4 tetrahedra. The surroundings of such TM ions would likely be an octahedron that consists of the apices of BO_4, because of the high field strength of the dopant ions.

The role of transition metal ions in sodium-borate glasses has been established to be essentially the same as that of the modifier Na^+.[9] The estimation of Racah parameters allows one to infer some aspects of the local structure of TM ions. Ions such as Cr^{3+} are said to have high ligand field stabilization energy.[4] This means that Cr^{3+} will attempt to satisfy its own bonding requirements with

respect to the coordinated ligands, resulting in a more symmetric arrangement in a regularly-bonded complex. The situation is likely quite different in a glass, however, as the high viscosity of the studied melts likely prohibits any ordering for Cr^{3+} with its neighboring oxygens.

The calculated B and C parameters are very reasonable for Mn^{2+} and are as expected, but Cr^{3+} shows a relatively high value of Dq and an extremely low value of B, approximately 300 cm^{-1}, which is well shifted from the value of the free ion. The conclusion is that Mn^{2+} assumes very similar surroundings almost regardless of the host material—the octahedral sites must be quite regular, as they correspond directly to the absorption and luminescence spectra predicted from theory and seen in crystals and solutions. It can be said that Mn^{2+} is in fact satisfying its own desire to be coordinated by a regular octahedron of oxygens (in BO_4 tetrahedra) in which the bonding is mostly ionic, but Cr^{3+} does not have the same influence on its surroundings as the glass is cooled from the liquid. The Cr^{3+} ions are likely 'stuck' in regions where the bonding interaction is more covalent with surrounding oxygens, preventing the regularity of the octahedral surroundings in the final structure of the glass.[8,9] The distorted octahedral sites of Al_2O_3:Cr allow strong luminescence, but chromium in the sodium-borate regions is in a distorted position that does not allow the energy level-separation that is required for ruby fluorescence, for example.[5]

Cr^{3+} offers interesting luminescence properties in various hosts (such as Al_2O_3, but the emission properties of the Cr^{3+} doped glass studied here do not offer much promise for the desired LED phosphor scheme. The absorbance and luminescence spectra correspond to roughly octahedral coordination of Cr^{3+} by oxygen, but the lack of intense emission places the crystal field on the lower energy side of the energy level diagram for the d^3 ion.[3,5] The Mn^{2+} ion on the other hand is able to attain an octahedral coordination in alkali borosilicates (and many other oxides as well) that is conducive to intense luminescence.

Less detail is known about the niobium glasses. Nb ions are likely situated in the same types of distorted octahedra as in crystals, but absorption and luminescence phenomena can not be ascribed to any of the known transitions

from energy level diagrams and ligand-field or molecular-orbital theory. However, the reduced samples show two different fluorescence transitions in the alkali borosilicate host upon short and long wave UV excitation.

A comparison of the present results with those for Mn^{2+} in binary alkali silicates shows the difference in the role of TM ions as modifiers. The binary alkali silicates contain more NBOs with more alkali additions, and the luminescence properties of Mn^{2+} in these glasses is dependent on the number of NBO—the red emissions are said to increase when the # of coordinated NBO increases.[8] The alkali borosilicate system studied in this work is quite different. The relatively high percentage of alkali in the glass is mostly associated with the borate phase, meaning that there are significant BO_4 units, but the number of NBO is difficult to discern without an appropriate model. The NBO are not likely to affect the observed luminescence of Mn^{2+}-doped alkali borosilicate glasses. It is more probable that the Mn^{2+} ions draw boron polyhedra toward them (field strength arguments) in cooling and set up a regular arrangement of BO_4 in their immediate vicinity. The stronger bonding of the BO_4 (as opposed to a glass with mostly BO_3 units) being surrounded by rigid SiO_2 glass, the possibility of regular octahedral arrangement, and the equal dispersion of the $Na_2O{\bullet}B_2O_3$ and SiO_2 phases in the glass are probably the most beneficial properties to the observed luminescence.

B. The Possibility of a Doped Glass Phosphor

The work performed to date shows that the idea of a glass phosphor/LED combination using transition metals is quite promising. The thermal properties of the alkali-borosilicate are quite near to what is desired optimally (moderate softening temperatures and low thermal expansion). The host glass composition may also be tailored further for T_g or CTE, depending on the exact application. The Mn^{2+} and Nb^{5+} ions do not color the glasses. The two reduced samples featured the appropriate high intensity luminescence upon excitation with long range UV/violet/blue light. It is of interest that their peak emission wavelengths are nearly the same (roughly 600-605 nm), which would require the use of other dopants (most likely rare earths such as Ce, Dy, Tb, Eu for the emission of

yellow, blue, or green) to achieve the necessary white-color rendering. The Cr^{3+} ions impart a heavy green color to the glass and offer a weak luminescent emission, so would not be suitable in frequency-conversion phosphor system. The transparency of glasses containing Mn^{2+} and $Nb^{4+/5+}$ would be very useful for focusing the LED beams and reduction of scattering. It has proven difficult to achieve the reduced states of manganese and niobium simultaneously via traditional batch-melting techniques. However, each ion offers promise as a single dopant in the alkali borosilicate to achieve orange emission from a long UV or blue source.

V. CONCLUSIONS AND SUGGESTIONS FOR FURTHER WORK

Both the alkali borosilicate host material and the transition metal ions studied offer high potential as frequency-shifting photoluminescent materials. The alkali borosilicate compositions show fairly low [CTE], which may be customized to match the desired expansion of gallium nitride LED materials. The onset of glass transition is also quite low for compositions 1-3, ranging from around 440 to 500° C. The thermal expansion of compositions 1 and 2 compare favorably with the gallium nitride materials. A direct-melt glass coating is not immediately foreseeable, but it may be possible to sinter a doped-glass frit to achieve a homogeneous glass phosphor coating.

Luminescence spectra of manganese and niobium show very broad emission bands that would benefit color-rendering. It has proven possible using traditional batching and melting techniques to reduce a typical alkali-borosilicate batch to obtain the reduced form of manganese (Mn^{2+}) which offers intense orange luminescence upon excitation with long-UV to blue light. Cr^{3+} likely occupies a highly-distorted octahedral site, and the luminescence in the studied host glass is not useful for the desired purpose. The absorption and emission bands of Mn^{2+} correspond to a fairly regular octahedral site. The irregularity of glass structures enables the presence of distorted niobium octahedra (due to the presence of $Nb^{4+/5+}$ and possibly Nb^{3+}) which are said to be responsible for the observed luminescence.

There may be other possibilities to supplement this work. Most of the observed optical properties are due to the local environments of the activator ions, so techniques to investigate this short-range order around these ions would be beneficial. Techniques such as extended x-ray absorption fine structure [EXAFS] may allow one to determine if there is a peak due to a shortened niobyl group present in the niobium octahedra, for example, or the degree of disorder present in Cr^{3+} and Mn^{2+} coordination polyhedra. Raman scattering spectroscopy may elucidate the possibility of the TM ions having some glass forming nature, as opposed to strict modifier behavior. Raman scattering has been used to show that

certain TM ions significantly affect silicate glass structures by substituting for Si^{4+} and occupying tetrahedral positions in the network.[9]

The choice of the alkali-borosilicate host was arbitrary, but this glass system has proven to be nearly ideal for the intended application. Additional glasses could be formulated to match exactly the expansion behavior of a specific InGaN compound, or further reduce T_g. In addition, P_2O_5 glasses are known as hosts for activator ions, and display a low onset of glass transition, but working with them is more difficult.

Indeed, the emission of Mn^{2+} ions is well understood, and their use in an alkali-borosilicate host offers a phosphor material that is potentially very cost effective. An additional requirement for white emission of suitable indoor spectrum would be the appropriate mix of rare-earth activators with Mn^{2+} in the described glass system. The rare earth ions generally attain a preferred oxidation state in a glass system (generally 3+) which is difficult to alter. It may be possible to produce Mn^{2+} in combination with the appropriate trivalent rare earth activators by traditional batching and melting techniques.

REFERENCES

1. G. Blasse and B.C. Grabmaier, *Luminescent Materials*. Springer-Verlag, Berlin, 1994.

2. C.J. Ballhausen, *Introduction to Ligand Field Theory;* pp. 200-83. McGraw-Hill, New York, 1962.

3. L.E. Orgel, *An Introduction to Transition Metal Chemistry: Ligand Field Theory*. Methuen, London, 1960.

4. A. Paul, *Chemistry of Glasses;* pp. 280-347. St. Edmundsbury Press, Bury St. Edmunds, UK, 1990.

5. K. Nassau, *The Physics and Chemistry of Color: The Fifteen Causes of Color*. John Wiley and Sons, New York, 2001.

6. S. Sugano, Y. Tanabe, and H. Kamimura, *Multiplets of Transition-Metal Ions in Crystals*. Academic Press, New York, 1970.

7. J.A. Caird and S.A. Payne, "Section I: Solid State Lasers," pp. 1-100 in *CRC Handbook of Laser Science and Technology.* Edited by M. J. Weber. CRC Press, Boca Raton, FL, 1991.

8. C. Nelson and W.B. White, "Transition Metal Ions in Silicate Melts--I. Manganese in Sodium Silicate Melts," *Geochim. Cosmochim. Acta,* **44** [6] 887-93 (1980).

9. C. Nelson, T. Furukawa, and W.B. White, "Transition Metal Ions in Glasses: Network Modifiers or Quasi-molecular Complexes?," *Mater. Res. Bull.,* **18** [8] 959-66 (1983).

10. L.J. Andrews, A. Lempicki, and B.C. McCollum, "Spectroscopy and Photokinetics of Chromium (III) in Glass," *J. Chem. Phys.,* **74** [10] 5526-37 (1981).

11. I.M. Batyaev, I.V. Golodova, S.V. Levshin, and S.B. Sukhanov, "Spectral Luminescent Properties of the Cr^{3+} Ion in Alkali-Phosphate Al_2O_3-P_2O_5-Me_2O-MeO Glasses," *Opt. Spectrosc.,* **78** [2] 228-30 (1995).

12. K. Bingham and S. Parke, "Absorption and Fluorescence Spectra of Divalent Manganese in Glasses," *Phys. Chem. Glasses,* **6** [6] 224-32 (1965).

13. D.L. Griscom, "Electron Spin Resonance in Glasses," *J. Non-Cryst. Solids,* **40** [1-3] 211-72 (1980).

14. R.V.S.S.N. Ravikumar, R. Komatsu, K. Ikeda, A.V. Chandrasekhar, B.J. Reddy, Y.P. Reddy, and P.S. Rao, "Electron Paramagnetic Resonance and Optical Absorption Spectra of Cr^{3+} Ions in Cadmium Phosphate Glass," *Solid State Commun.,* **126** [5] 251-3 (2003).

15. J.H. Yum, S.Y. Seo, S. Lee, and Y.E. Sung, "$Y_2Al_5O_{12}:Ce_{0.05}$ Phosphor Coatings on Gallium Nitride for White Light Emitting Diodes," *J. Electrochem. Soc.,* **150** [2] H47-H52 (2003).

16. W.D. Fragoso, C.D.M. Donega, and R.L. Longo, "Luminescence and Energy Transfer in La_2O_3-Nb_2O_5-B_2O_3: M^{3+} (M = Bi, Eu, Dy) Glasses," *J. Lumin.,* **105** [2-4] 97-103 (2003).

17. K.J. Lynch, "Fluorescence of Cr^{3+}, $Mn^{2+/3+}$, and Eu^{3+} in High Alkali Zinc Borosilicate Glass Used in Electroluminescent Devices"; M.S. Thesis. Alfred University, Alfred, NY, 2002.

18. J. Wong and C.A. Angell, "Electron Paramagnetic Resonance in Glass," pp. 555-668 in *Glass Structure by Spectroscopy.* Marcel Dekker, New York, 1976.

19. E.J. Friebele and D.L. Griscom, "Radiation Effects in Glass," in Treatise on Materials Science and Technology, Vol. 17, *Glass II.* Edited by M. Tomozawa and R. H. Doremus. Academic Press, New York, 1979.

20. D.M. Krol and G. Blasse, "The Influence of the Li/Nb Ratio on the Luminescence Properties of $LiNbO_3$," *J. Chem. Phys.,* **73** [1] 163-6 (1980).

21. A.J.H. Macke, "Luminescence in the System $Mg_4Ta_{2-x}Nb_xO_9$," *J. Solid State Chem.,* **19** [3] 221-6 (1976).

22. A.M. Srivastava, J.F. Ackerman, and W.W. Beers, "On the Luminescence of $Ba_5M_4O_{15}$ (M = Ta^{5+}, Nb^{5+})," *J. Solid State Chem.,* **134** [1] 187-91 (1997).

23. G. Hochstrasser, "Detection of VO^{2+} in Glass by Electron Spin Resonance," *Phys. Chem. Glasses,* **7** [5] 178-82 (1966).

24. A. Paul and F. Assaghby, "Optical and ESR Spectra of Vanadium (IV) in Different Simple Germanate, Phosphate, and Borate Glasses," *J. Mater. Sci.,* **10** [1] 613-20 (1975).

25. C. Kittel, *Introduction to Solids State Physics;* pp. 461-90. John Wiley and Sons, Singapore, 1986.

26. Y.M. Kim, D.E. Reardon, and P.J. Bray, "ESR Studies of Radiation-Induced Niobium Centers in Nb_2O_5-Na_2O-SiO_2 Glasses," *J. Chem. Phys.,* **48** [8] 3396-402 (1968).

27. J.E. Shelby, *Introduction to Glass Science and Technology;* pp. 1-211. The Royal Society of Chemistry, Cambridge, 1997.

28. A.K. Varshneya, *Fundamentals of Inorganic Glasses;* pp. 75-85. Academic Press, New York, 1994.